AE in Masonry

Springer Book

Acoustic Emission Testing

Edited by Christian U. Grosse, Masayasu Ohtsu, Dimitrios Aggelis, Tomoki Shiotani

Chapter 15 "AE in Masonry"

Els Verstrynge[†], Giuseppe Lacidogna[*], Federico Accornero[*]

[†]*KU Leuven, Civil Engineering Department, Building Materials and Building Technology Section, Kasteelpark Arenberg 40, 3001 Heverlee, Belgium.*

**Politecnico di Torino, Department of Structural, Geotechnical and Building Engineering, Corso Duca degli Abruzzi 24, 10129 Torino, Italy.*

Contents

15 AE in masonry

15.1 Introduction

Since Acoustic Emission (AE) is a non-invasive and non-destructive monitoring technique, it is ideally suited for use in the assessment of historic masonry structures that are subjected to high sustained loads (Verstrynge, Schueremans et al., 2009; Verstrynge & Van Gemert, 2018), or, are exposed to seismic risk (Carpinteri & Lacidogna, 2007a, 2007b, 2008; Carpinteri, Lacidogna, Invernizzi et al., 2013). Having identified the fractured or damaged portion of a structure, it is possible to evaluate its stability from the evolution of damage, which may either gradually come to a halt or propagate at an increasingly fast rate (Behnia, Chai et al., 2014; Carpinteri & Lacidogna, 2006a, 2006b; Shiotani, Fujii et al., 1994; A. K. Tomor & Verstrynge, 2013; Verstrynge, 2019). Moreover, if the position of the defects is not known to begin with, it can be located by making use of a multiplicity of sensors and by triangulation techniques, prior to assessing the stability of a structure based on the evolution of damage phenomena (Carpinteri, Lacidogna et al., 2006; Grosse, Reinhardt et al., 1997; Lacidogna, Manuello et al., 2015; Shah & Li, 1994). The purpose of this chapter is therefore to highlight the strengths and pitfalls of using the acoustic emission technique for damage assessment in masonry structures, focusing as well on experimental work as on case studies with in-situ monitoring.

AE wave propagation in masonry suffers from high attenuation and signal distortion due to the relatively low density and high heterogeneity of the material. In general, AE wave velocities are usually larger in bricks and blocks, compared to the mortar joints. In addition, the brick-mortar interfaces, cracks and different layers of multi-leaf walls might act as reflection surfaces. Since the AE signal characteristics are influenced by the wave propagation path and the distance between source and sensor, AE signal analysis and AE source location in masonry structures are not straightforward. In many reported test campaigns, the source localization is

performed by considering the position of the sensor that firstly detected the AE hit, as detection ranges are relatively low. In addition, it will be shown in this chapter that analysis of AE results for masonry structures is more commonly based on a statistical interpretation of AE data rather than analysis of the individual AE burst signal characteristics.

In this chapter, firstly an overview is presented of AE analysis techniques for damage detection in masonry, with specific reference to the issues that complicate AE sensing in masonry as described above. These techniques extend the analysis approaches that were addressed in Part A of this book, and introduce some additional novel findings such as relations between damage state and $1/f$ noise power spectra, and effects of mortar joint crossings on AE signal parameters. Secondly, an overview of the authors' experience with on-site AE monitoring in historical masonry structures is presented and illustrated with several case studies. Finally, AE monitoring during experimental campaigns, with AE-based prediction of creep and fatigue failure and a comparison of AE results with other crack measurement techniques during a test on a full-scale masonry wall, is presented.

15.2 AE analysis for damage assessment in masonry

15.2.1 Statistical analysis of cumulative AE data

Acoustic emission data can be interpreted by means of statistical and fractal analysis, considering the multiscale aspect of cracking phenomena. This approach has shown that the energy emission, detected by AE, occurs in a fractal (lacunar) domain with a dimension lower than 3.0. Consequently, a multiscale criterion to predict the damage evolution has been formulated (Carpinteri, Lacidogna et al., 2007). Recent developments in fragmentation theories have shown that the energy W during micro crack propagation is released over a fractal domain comprised between a surface and

the specimen volume V (Carpinteri, Lacidogna et al., 2007). As a result, the following size-scaling law has been assumed for the energy release W during fragmentation:

$$W \propto V^{D/3}, \tag{1}$$

where D is the so-called fractal exponent, comprised between 2.0 and 3.0. There are numerous evidences on the dependence of the fractal exponent D from the conditions of fragmentation. Catastrophic failure under compression would be associated to low D values approaching to 2.0, whereas extensive crushing under compression would generate higher D values, close to 3.0.

As a consequence of Eq. (1), the energy density scales as:

$$\Psi = \frac{W}{V} \propto V^{(D-3)/3}. \tag{2}$$

This implies that not the true energy density but a fractal energy density (having non-integer physical dimensions) can be considered as the size-independent parameter:

$$\Gamma = \frac{W}{V^{D/3}}, \tag{3}$$

On the other hand, during micro crack propagation, AE can be clearly detected. The energy emission W is proportional to the number N of AE events. Accordingly to the energy release from a fractal domain, as described by Eq. (3), the number of AE events, N, not over a volume but over a fractal domain, can be considered as the size-independent parameter:

$$\Gamma_{AE} = \frac{N}{V^{D/3}}, \tag{4}$$

where Γ_{AE} is the value of AE events fractal density. The fractal criterion in Eq. (4) permits to extend Eq. (1) as follows:

$$W \propto N \propto V^{D/3}. \tag{5}$$

Moreover, a statistical interpretation to the variation of the b-value during the evolution of damage detected by AE has been proposed, which is based on a treatment originally proposed by Carpinteri and co-workers (Carpinteri, Lacidogna, Accornero et al., 2013; Carpinteri, Lacidogna, & Manuello, 2009). The proposed

model captures the transition from the condition of diffused criticality to that of imminent failure localization.

By analogy with seismic phenomena the magnitude of AE signals may be defined as follows:

$$m = Log_{10} A_{\max} + f(r) \tag{6}$$

where A_{max} is the amplitude of the signal expressed in volts, and $f(r)$ is a correction taking into account that the amplitude is a decreasing function of the distance r between the source and the sensor.

In seismology the empirical Gutenberg-Richter's law:

$$Log_{10} N(\geq m) = a - bm \text{, or } N(\geq m) = 10^{a-bm}, \tag{7}$$

expresses the relationship between magnitude and total number of earthquakes in any given region and time period, and it is one of the most widely used statistical relations to describe the scaling properties of seismicity. In Eq. (7), N is the cumulative number of earthquakes with magnitude $\geq m$ in a given area and within a specific time range, whilst a and b are positive constants varying from one region to another and from one time interval to another. Equation (7) has been used successfully in the AE field to study the scaling laws of AE wave amplitude distribution. This approach evidences the similarity between structural damage phenomena and seismic activities in a given region of the Earth's crust, extending the applicability of the Gutenberg-Richter's law to Structural Engineering. According to Eq. (7), the b-value changes systematically at different times in the course of the damage process and therefore can be used to estimate damage evolution modalities.

Equation (7) can be rewritten in order to draw a connection between the magnitude m and the size L of the defect associated with an AE event. By analogy with seismic phenomena, the AE crack size-scaling entails the validity of the relationship:

$$N(\geq L) = cL^{-2b}, \tag{8}$$

where N is the cumulative number of AE events generated by source defects with a characteristic linear dimension $\geqslant L$, c is a constant of proportionality, and $2b = D$ is the fractal dimension of the damage domain.

Aki (Aki, 1981) was the first to show that the seismic b-value is related to the fractal dimension D, and that usually $2b = D$. This assumption −and its implication with the damage energy release rate and time dependent mechanisms, both at the laboratory and at the Earth's crust scale− has been also pointed out by Main (Main, 1991). Moreover, it has been evidenced that this interpretation rests on the assumption of a dislocation model for the seismic source and requires that $2.0 \leq D \leq 3.0$, i.e., the cracks are distributed in a fractal domain comprised between a surface and the volume of the analyzed region.

The cumulative distribution in (8) is substantially identical to the cumulative distribution which gives the probability of a defect with size $\geq L$ being present in a body (Carpinteri, Corrado et al., 2013):

$$P(\geq L) \propto L^{-\gamma}. \tag{9}$$

Therefore, the number of defects with size $\geq L$ is:

$$N^*(\geq L) = c\, L^{-\gamma} \tag{10}$$

where γ is a statistical exponent measuring the degree of disorder, i.e. the scatter in the defect size distribution, and c is a constant of proportionality. By equating distributions (8) and (10) it is found that: $2b = \gamma$. At the collapse, the size of the maximum defect is proportional to the characteristic size of the structure. As shown by Carpinteri and co-workers (Carpinteri, Corrado et al., 2013), the related cumulative defect size distribution (referred to as self-similarity distribution) is characterized by the exponent $\gamma = 2.0$. It was also demonstrated that $\gamma = 2.0$ is a lower bound which corresponds to the minimum value $b = 1.0$, observed experimentally when the load bearing capacity of a structural member has been exhausted. Therefore, by determining the b-value, it is possible to identify the energy emission modalities in a structural element during the monitoring process. The extreme cases envisaged by

Eq. (5) are D = 3.0, which corresponds to the critical conditions b = 1.5, when the energy emission takes place through small defects homogeneously distributed throughout the volume, and D = 2.0, which corresponds to b = 1.0, when energy emission takes place on a fracture surface. In the former case, diffused damage is observed, whereas in the latter, two-dimensional cracks are formed leading to the separation of the structural element.

15.2.2 Damage assessment under cyclic loading

Under cyclic loading, the LOAD-CALM analysis method, as presented elsewhere in this book, is often applied in masonry. The LOAD ratio, also known as the Felicity ratio, indicates the ratio between the load at the start of AE activity in a current cycle and the maximum load in a previous cycle. A ratio of 1.0 represents the Kaiser effect, often referred to as the "memory of the material". Upon the occurrence of internal damage in the material's micro structure, the ratio drops below 1.0. The CALM ratio represents the AE activity during the unloading phase and is therefore also an indication of the presence of internal defects. Hence, both ratios can be combined to assess the damage state. In masonry, this approach is particularly useful as it compares AE activity in subsequent cycles of a load test on a structure. Hence, these ratios are less affected by the high attenuation in masonry, as would be the case for other parameters such as amplitude and energy.

Cyclic three-point bending tests were performed on blocks of refractory masonry by Andreev at al. (Andreev, Shetty et al., 2018). It was found that the LOAD-CALM analysis allowed differentiating the fracture progress in refractories of various brittleness and the AE-based damage limits from cyclic testing were related to the fatigue limits of the respective refractory materials. In (Shetty, Livitsanos et al., 2019), LOAD-CALM analysis was performed on masonry walls with various mortar types under cyclic compressive loading, see **Fig. 15.1**. By comparing acoustic emission analysis and digital image correlation, Shetty et al. found that the damage

limits established for AE-based assessment of concrete in bending, were too conservative for masonry structures under cyclic loading. An on-site load test on a historical masonry vault was performed by Carpinteri et al. (Carpinteri, Invernizzi et al., 2006). The test loading was carefully applied by means of water cushions, and AE counts were reported. Interestingly, AE activity was reported to start only upon exceedance of the previously reached maximum load level. This signifies an on-site recording of the Kaiser effect on a masonry vaulted structure. In Section 15.4.2, the application of Felicity ratio during lab experiments on a full scale masonry wall will be presented.

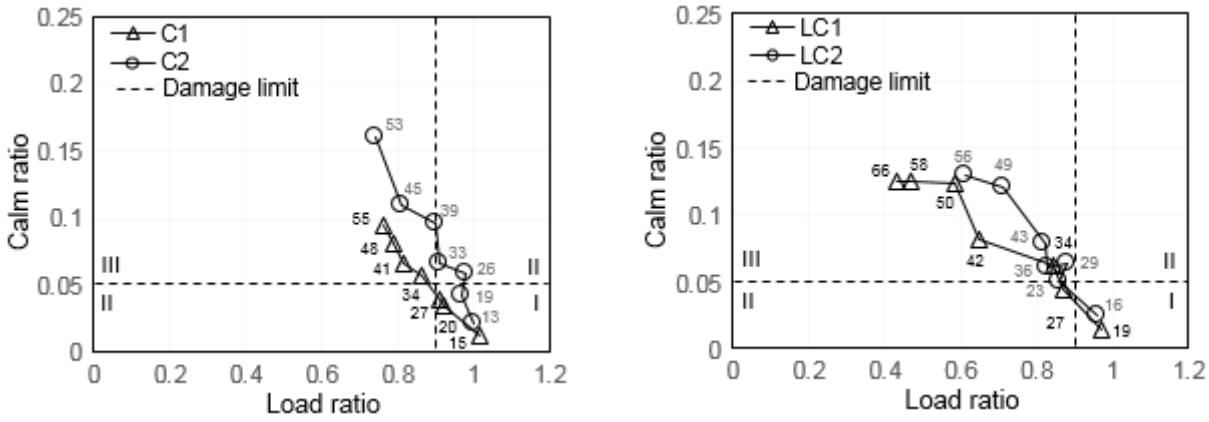

(a) (b)

Fig. 15.1 Load-Calm ratios for two masonry walls with (a) cement mortar, (b) lime-cement mortar. Zone I indicates minor or no damage, II intermediate damage, III heavy damage. Values are normalized compressive loads. Figures adopted from (Shetty, Livitsanos et al., 2019)

15.2.3 AE source location in orthotropic materials

Localization of acoustic emission sources in masonry is hindered by the heterogeneity of the material, giving cause to different propagation velocity of the elastic wave in different directions. Secondly, the high wave attenuation of the porous material reduces the maximum source-sensor distance. Generally, AE wave velocities

are higher in bricks and blocks, compared to the mortar joints for historical masonry. In addition, the brick-mortar interfaces will act as reflection surfaces. Therefore, AE source location based on a simple triangulation technique, which takes into account sensor setup, average velocity, and AE hit arrival time, is not straightforward in masonry. In many reported test campaigns, the source location is obtained by considering the location of the sensor that first detected the AE hit, as detection ranges are relatively low. Since existing cracks and voids further hinder the propagation of the AE signal, a detection range analysis is recommended for each sensor during on-site monitoring.

In recent studies by Livitsanos et al. (Livitsanos, Shetty et al., 2018a), it was shown that taking into account an orthotropic wave velocity in masonry largely increases the accuracy of the AE source location when applying triangulation techniques, see **Fig. 15.2**. The experiment concerned solid clay bricks and mortar with a hybrid lime-cement binder. These improved source location results were obtained by considering the elastic wave velocity along the bed joints to be almost double of the velocity perpendicular to the bed joints, since it was found that an increase in number of mortar joint crossings reduced the wave velocity.

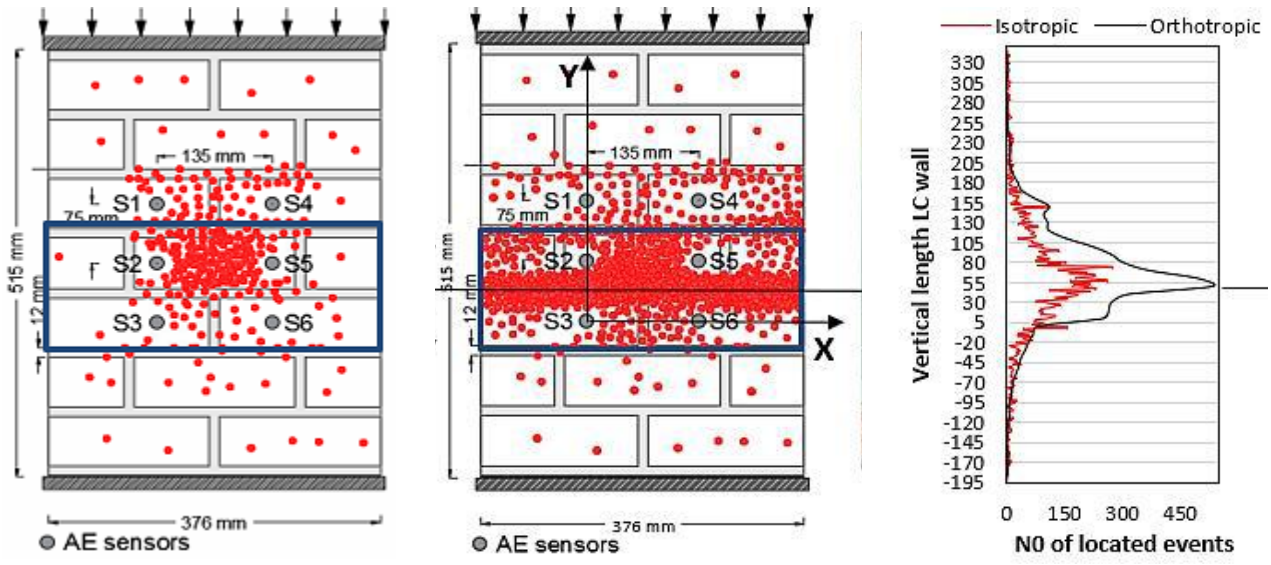

(a) (b) (c)

Fig. 15.2 Result of planar AE source location with isotropic (a) and orthotropic (b) wave velocity distribution. Red dots indicate located sources. The central mortar joint (indicated in the middle of the rectangle) was crushed during the compression test. (c) distribution of located AE events along the height of the masonry sample. Figures adopted from (Livitsanos, Shetty et al., 2018a)

15.2.4 Fluctuations of 1/*f* noise in damaged structures

The presence of power laws in critical phenomena seems to indicate that something deep appears in the spectral density of the so-called flicker noise, that is actually rather variable (Carpinteri, Lacidogna et al., 2018). It runs like $1/f^{\gamma}$, where $0.5 \leq \gamma \leq 1.5$, over different frequency magnitude orders. In particular, $1/f$ noise is associated to a signal whose spectrum is linear in a logarithmic scale. A color name, "pink noise", is given by analogy with pink light, which has such a linear power spectrum over the visible range. More generally, different colors are associated to noise with spectral profiles other than pink noise ($\gamma = 1$), in reference to the light with analogous spectra, e.g., the spectral density of white noise is flat ($\gamma = 0$), while red (or Brownian) noise has $\gamma = 2$.

Curiously enough, $1/f$ noise is present in nature in very unexpected places, i.e., the flow of the river Nile, the luminosity of stars, the loudness of a piece of classical music versus time, the flow of sand in an hourglass, and many others.

A crucial feature of $1/f$ noise is its scale invariance for any frequency or time range, and for this reason it has been considered as a wide manifestation of the fractal character of several natural phenomena. The concept of scaling, which leads to power laws, is present also in the physics of earthquakes (Carpinteri, Lacidogna, Accornero et al., 2013). Moreover, it can be observed that even in quasi-brittle materials, like rocks, concrete, and masonry, there is a source of $1/f$ noise in AE from fracture phenomena. The results of laboratory tests performed on specimens of rocks and

concrete, and of in-situ monitoring of Italian historical buildings (Carpinteri, Lacidogna et al., 2018) show how, representing the obtained AE data in a log-log plot of spectral density versus frequency, a $1/f$ noise behavior is meaningful also in damaging structures. Summarizing the frequency fluctuation data obtained by compression tests carried out in lab tests (Carpinteri, Lacidogna et al., 2018) proves that, before the achievement of the peak load, AE signals reveal a source noise basically "white" ($1/f^{0}$) that is characteristic of prominent random phenomena. On the contrary, after peak load, the source noise revealed by AE signals is characterized as "pink" ($1/f^{1}$), that is distinctive of correlated phenomena.

In fact, before the critical state is reached, when the damage is characterized by the formation of micro cracks uniformly distributed in the structure, and the dominant fracture surfaces have not yet been generated, the energy emitted from the material and measured through AE signals is characterized by small variations for every frequency range. The distribution of micro cracks is therefore random and evenly distributed in the damaged body. On the other hand, preferential fracture surfaces are generated after the critical state, and then the energy emitted by the damaged material is characterized by significant variations in relation to the frequency: the lower the signal frequency, the higher the emitted energy by the damaged body. In this case, the AE sources appear distributed on preferential fracture surfaces.

The interpretation of $1/f$ noise phenomena through the use of the AE technique can be therefore very useful for identifying the transition from the critical conditions of a structure to those that involve an incipient collapse.

15.2.5 Remarks concerning AE signal analysis in masonry

Most techniques mentioned above rely on AE event counting and analysis of the cumulative AE activity. When applying crack classification methods, based on signal

parameters such as frequency, amplitude and duration, the effects of distortion of the ultrasonic waves has to be taken into account (Aggelis, Mpalaskas et al., 2012; Carpinteri, Lacidogna, Accornero et al., 2013). In masonry, the distortion of the wave properties increases with increasing source-sensor distance and number of mortar joint crossings. In **Fig. 15.3**, the effect of an increasing wave propagation path on Average Frequency (AF) and Rise Time (RT) in masonry is shown (Livitsanos, Shetty et al., 2018b). Both experimental and numerical results are consistent and show an increase in RT and slight decrease in AF. This is in agreement with similar studies on cementitious mortar samples (Aggelis, Mpalaskas et al., 2012), while the distortion effect increases with the amount of cracks, voids and interfaces. Since both parameters, RT and AF, are often applied in distinguishing tensile and shear mode fracture (see elsewhere in this book), source-sensor distance should be limited and/or distortions should be compensated when crack classification is aimed at in masonry structures.

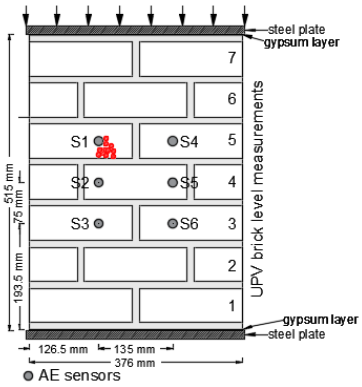

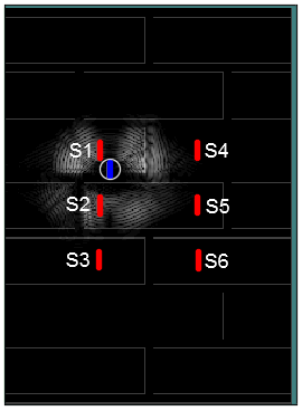

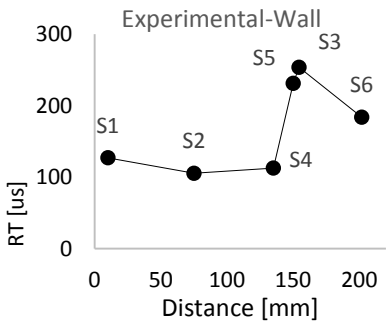

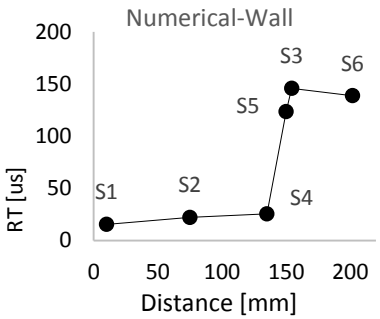

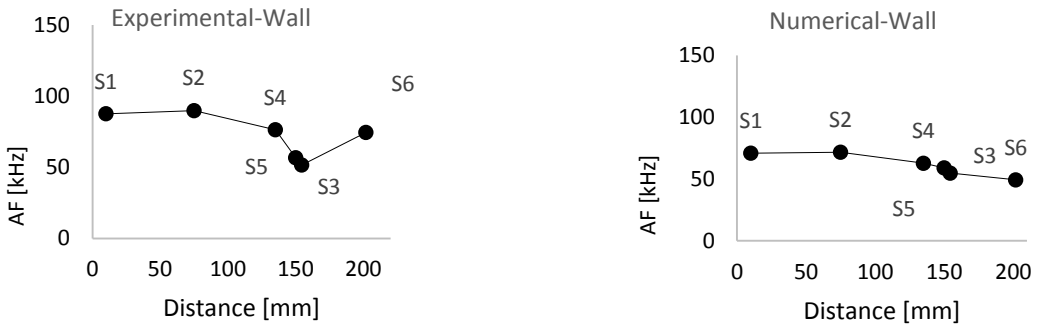

(a) (b)

Fig. 15.3 Effect of propagation distance on Rise Time (RT) and Average Frequency (AF), obtained from (a) AE events located near sensor 1 (S1) during a compression test, and (b) AE events simulated near sensor 1 (S1) in a numerical analysis. Figures adopted from (Livitsanos, Shetty et al., 2018b)

15.3 AE monitoring of historical buildings and monuments

Using the AE technique, the authors have acquired considerable experience in the monitoring of historical buildings and monuments (Anzani, Binda et al., 2008; Carpinteri & Lacidogna, 2006a, 2006b, 2007a, 2007b, 2008; Carpinteri, Lacidogna, Invernizzi et al., 2009; Carpinteri, Lacidogna, & Manuello, 2009; Niccolini, Carpinteri et al., 2011). In this Section, different case studies are presented to show the AE technique's capability on the assessment of damage evolution in ancient brick and stone monuments. All the analyzed structures are located in remarkable Italian sites from the Architectural Heritage point of view.

As a first example, AE monitoring is used on the masonry structure of an historical building, "Casa Capello", located in the center of the Rivoli Municipality (near Turin), to evaluate the development of the cracking phenomena which had been observed in a number of structural parts after the collapse of a breast wall on the downhill side of the building. With the measurement system adopted, entailing no

loading or invasive procedures, it proved possible to predict the arrest of crack growth and the onset of a new stability condition (Carpinteri & Lacidogna, 2006a).

Secondly, an interesting study is focused on the structural stability of three medieval towers, “Torre Sineo”, “Torre Astesiano” and “Torre Bonino”, rising in the center of Alba, a characteristic town in Piedmont. The damage processes in some portions of the masonry are monitored using AE sensing, making it possible to estimate the amount of energy emitted during the fracture process and to obtain information on the criticality of ongoing processes (Carpinteri & Lacidogna, 2007a). Moreover, the impact of earthquakes on damage evolution is assessed for all the towers (Carpinteri & Lacidogna, 2006b).

Thirdly, another original application of the AE technique concerns the evaluation of the state of conservation of mural paintings and their structural supports. This study in particular focuses on the painting surfaces of the Monte Tabor Chapel, in the UNESCO Renaissance Complex of the Sacred Mountain of Varallo, in Piedmont (Carpinteri, Lacidogna, Invernizzi et al., 2013).

Finally, several cases studies are briefly discussed that illustrate the evaluation of the *b*-value and 1/*f* noise power spectra to assess the criticality of fracture. Among these case studies is the Asinelli Tower in Bologna (Carpinteri, Lacidogna et al., 2016).

For the on-site monitoring campaigns, the leading-edge equipment adopted by the authors consists of six "Units for Storage Acoustic emission Monitoring" (USAM) that can be synchronized for multichannel data processing (Anzani, Binda et al., 2008; Carpinteri, Lacidogna, Accornero et al., 2013; Carpinteri, Lacidogna, Invernizzi et al., 2009; Carpinteri, Lacidogna, & Manuello, 2009; Niccolini, Carpinteri et al., 2011). The most relevant parameters acquired from the AE signals (frequencies in a range

between 50 and 800 kHz, arrival time, amplitude, duration, number of events and oscillations) are stored in the USAM memory and then downloaded to a PC for multi-channel data processing. Micro cracks localization is performed by triangulation and the damage condition of the monitored specimen is determined.

15.3.1 "Casa Capello" historical masonry building

The historical building known as "Casa Capello" is presently a hospice for elderly people (**Fig. 15.4**). Interventions were carried out for its restoration and functional extension in the years 1996-1999. The building rises in an area situated in the historical center of Rivoli, near Turin (Italy), delimited by Via alla Parrocchia and Via Stella Maris, approximately half way between the Rivoli Castle hill and the valley floor. The building, which looks onto the Medieval Church of the Collegiata, was erected on pre-existing foundations dating back to the 14th Century and was drastically restructured in the 18th Century, when it acquired its present appearance. The main construction is a masonry building which follows the slope of the land and has three storeys facing the streets and two storeys looking onto the inner courtyard. The restoration works performed on this complex took into account its historical and architectural values and respected its sober styling by making changes and additions that blended in with the existing volumes.

Fig. 15.4 “Casa Capello” in Rivoli (Turin); in the background the bell tower of the Collegiata, in the foreground the breast wall that collapsed during the restoration works.

The building reflects the classical design of 18th Century masonry structures. The original body, along Via Stella Maris, has partition walls which determine a box-like resisting frame specially designed to distribute the loads evenly (**Fig. 15.5**). The thickness of the masonry walls is constant throughout, from the basement to the third floor above ground, and always at least 60 cm. The walls are made of bricks, of average size for Italian historical buildings (about 5.5x12.5x25 cm), with interposed mortar joints ca 1 cm thick. The distribution of the windows, on the front, is regular, with no discontinuity (**Fig. 15.6**). The roof structure consists of solid wooden beams.

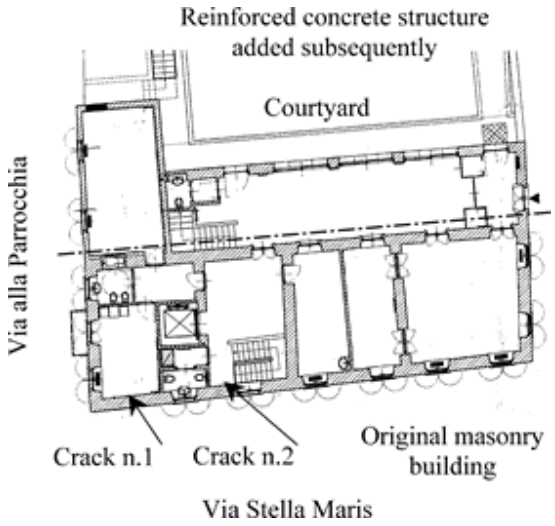

Fig. 15.5 Plan of the building

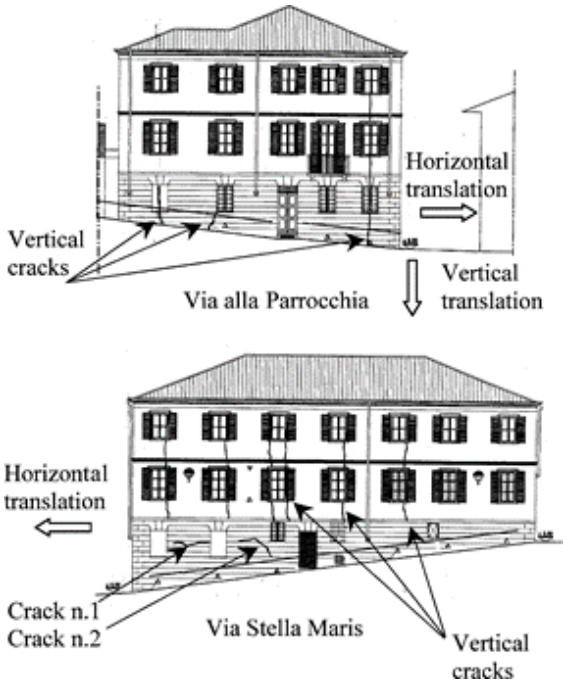

Fig. 15.6 Views of the building with the respective crack configurations

During the restoration works of "Casa Capello", an unexpected accident caused a partial collapse of the breast wall on the downhill side of the building, which altered the equilibrium of the substructures. The damages were immediately repaired by reconstructing the breast wall and strengthening the soil under the wall. Nevertheless, following the accident, a diffused network of cracks began to form in the masonry of the original building structure, with capillary fissures propagating through the masonry front.

The cracks are particularly evident in the masonry walls facing Via Stella Maris and Via alla Parrocchia (**Fig. 15.6**). On the building facade looking on Via Stella Maris, the cracks reveal a predominantly vertical pattern affecting the weakest zones of the masonry at the windows. On the internal surface of the same structure, two noticeable cracks appeared, following a horizontal pattern, about 1.8 m above the basement floor. The first (crack n. 1) opened in a room about 2 m from the corner of the building; the second (crack n. 2) in an adjacent staircase room, about 2 m from the first. These two

cracks propagated slowly, and therefore it was possible to monitor them by means of the Acoustic Emission technique (**Fig. 15.7**). The cracking pattern in the masonry facades along Via Stella Maris and Via alla Parrocchia can be accounted for by assuming a relative translation of the terminal portions of either sides of the facades, due to the subsidence of the edges of the building brought about by the collapse of the breast wall (Carpinteri & Lacidogna, 2006a).

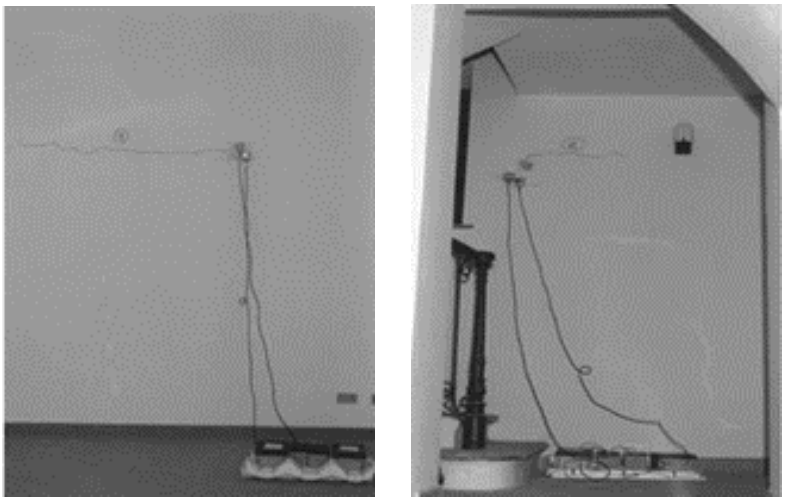

Fig. 15.7 Cracks n. 1 and n. 2 in the inner wall; PZT transducers placed at the tip of the cracks and AE monitoring equipment.

The evolution of crack n. 1 was monitored over a total of about 900 h, as specified in **Fig. 15.8**. The same figure also shows the trajectory of the crack at the time of initial application of the measuring system and the growth of the crack, expressed in cm. As can be seen, the crack displays a nearly horizontal development and retains a constant opening of about 0.2 mm during its evolution. The wall in which this crack developed, including the external plaster, was about 60 cm thick and was made of bricks with mortar joints of about 1 cm. During the strengthening works, a concrete wall ca 5 cm thick was built adjacent to the inner face of the masonry in order to improve the compressive strength of the wall. To collect the AE signals, two transducers were applied with their centers of gravity at ca 3 cm from the crack tip (to reduce the signal

attenuation due to the distance) (**Fig. 15.7**). A diagram illustrating the cumulative counting of AE events measured during the monitoring period is shown in **Fig. 15.9**. This curve is juxtaposed to the curve illustrating crack growth in mm. All the signals with an amplitude equal to or exceeding the 100 μV threshold, detected by the transducers during each monitoring stage, have been taken into account. The data plotted in the diagram has been determined from the average values obtained from the pair of transducers. As can be seen from the diagram, the counting number is proportional to the growth of the crack during every phase of the monitoring process and the fading of the counting rate clearly denotes the arrest of crack propagation. The same diagram also shows that the maximum counting rate was recorded when the velocity of crack growth was highest. After this event, the counting number and crack velocity quickly decreased to zero. Hence, it can be inferred that the peak of the AE distribution corresponded to the most critical period of crack growth. Then the crack approached a stability condition, as it progressed towards the compressed zones of the masonry. The effectiveness of the monitoring method is also due to the fact that the crack evolved slowly, at an average velocity of ca 0.04 mm/h, and developed in an area very close to the sensors. If it had propagated rapidly and moving away from the sensors, many signals might have escaped detection due to the attenuation effect.

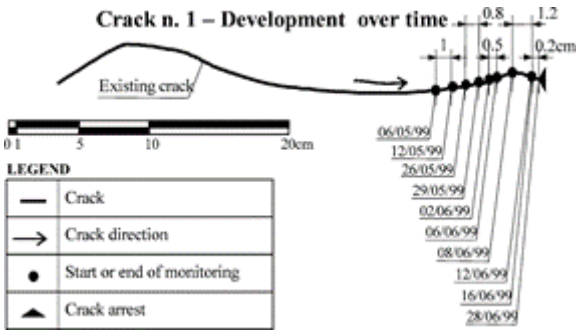

Fig. 15.8 Evolution of crack n. 1

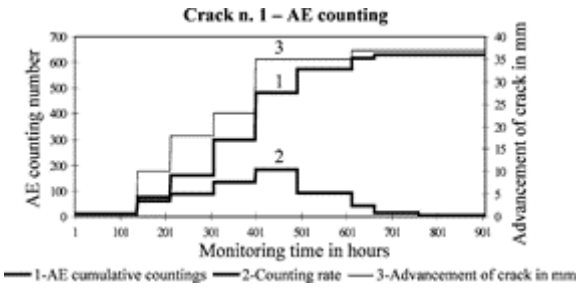

Fig. 15.9 Crack n. 1 monitoring results

Crack n. 2 was monitored over a total of ca 800 h. **Fig. 15.10** illustrates the development of the cracking pattern over time. In this case, we can see that the crack, after running horizontally over some distance, has undergone an oblique deviation, maintaining a constant width of about 0.2 mm throughout its development. The masonry where this second crack developed is 60 cm thick, is made of bricks and does not show any additional consolidation work. For the monitoring of crack n. 2, a pair of transducers placed at 3 cm from the crack tip (**Fig. 15.7**) was also used. As in the previous case, during each monitoring stage, the oscillations count considered all the signals having an amplitude equal to or exceeding the 100 μV. Again, the crack evolved very slowly at an average velocity of 0.17 mm/h. In this case too, we observe that the cumulative counting number is approximately proportional to the growth of the crack and that crack arrest coincides with the damping of the significant oscillations (**Fig. 15.11**).

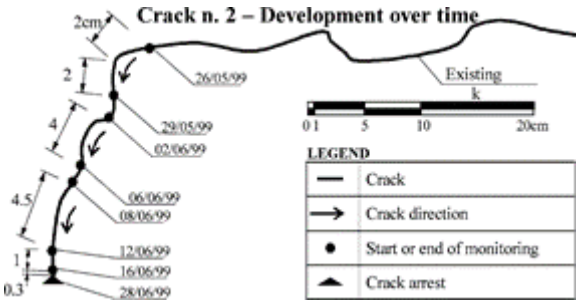

Fig. 15.10 Evolution of crack n. 2

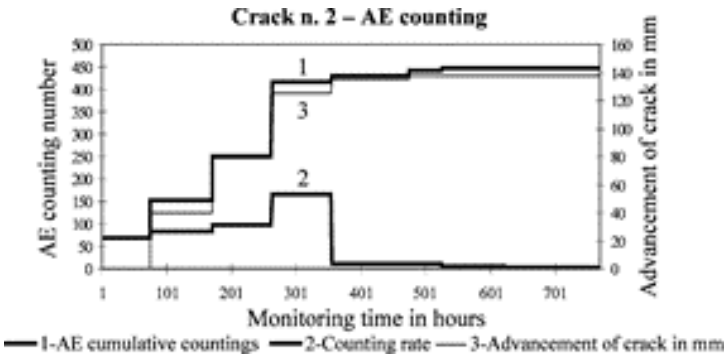

Fig. 15.11 Crack n. 2 monitoring results

The emission rate confirms that the maximum number of oscillations coincides with the maximum growth rate of the crack. Subsequently, a deceleration takes place and the counting rate, as well as crack velocity, quickly decrease to zero. The crack growth vs. time diagram shows a final stage denoting a stable behavior, the same as is observed in the diagram of cumulative AE counting versus time.

In a loading process involving the propagation of a crack, even if the attenuation due to the distance of perception of the signals is overlooked, the energy measured by the AE technique through the oscillations count is proportional to the energy emitted during the damaging process. Correlation diagrams (independent of time) between crack growth and the number of AE events recorded are shown in **Fig. 15.12**. In this manner, the behavior of the two masonry structures during the cracking process can be compared at glance. It can be seen that, over the same length, crack n. 2 emitted much less energy than crack n. 1, indicating that the toughness of the material where it developed was greater. For crack n. 2, the correlation values between crack growth and number of AE events are farther from the average line than the values obtained for crack n. 1. A higher scatter shows that the material crossed by crack n. 2 (bricks masonry) is more heterogeneous and therefore tougher, in the sense that it absorbs more energy, than the material crossed by crack n. 1 (the thin concrete wall).

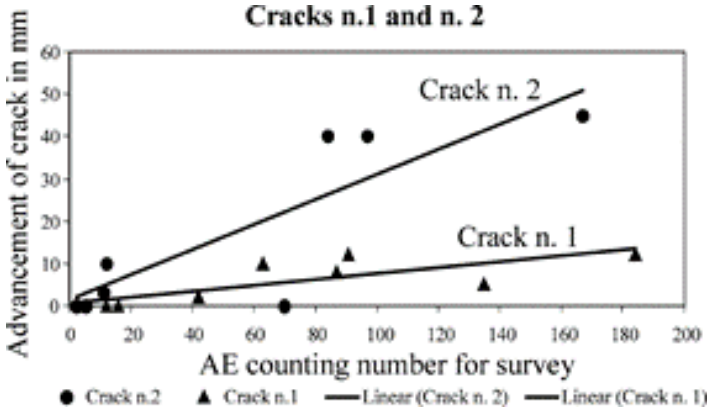

Fig. 15.12 Number of AE events vs. crack growth

In brief, by correlating the evolution of the cracks with the cumulative counting of AE events, we ascertained that crack growth underwent a progressive deceleration as the cracks progressed towards the compressed zones of the masonry, up to total arrest. The AE monitoring method was able to predict that the building structure would reach stability conditions with crack arrest. This monitoring method that compares the extent of structural damage with the energy emitted during crack propagation is easy to use and proves particularly effective in the case of slow propagation. In this case, in fact, by placing the sensors near the crack tip it becomes possible to avoid the attenuation effects due to the distance between the source and the receiver apparatus, which might entail the possible loss of AE signals.

15.3.2 The medieval towers of Alba

The medieval towers of Alba have been monitored by the AE technique. These masonry buildings from the 13th Century are the tallest and mightiest medieval towers preserved in Alba (**Fig. 15.13**). Torre Sineo is square, 39 m high, and leans to a side by about 1% (**Fig. 15.14**). Wall thickness ranges from 2 m at the foundation level to 0.8 m at the top. The bearing walls are constructed “a sacco”, i.e., consist of brick faces enclosing a mixture of rubble and bricks bonded with lime and mortar. Over a height of 15 m, the tower is incorporated in a later building. Torre Astesiano (**Fig.**

15.15) has a similar structure, but has a rectangular base. The filling material is more organised, with brick courses arranged in an almost regular fashion, which, however, are not connected with the outer wall faces. In this case, too, the total thickness of the masonry ranges from 2 m at the bottom to 0.8 m at the top. Total height is about 36 m and the tower does not lean predominantly on any side. It is also incorporated in a later building, approximately 15 m high, built when the tower had been completed. Torre Bonino (**Fig. 15.16**), just under 35 m high, is the least imposing of the towers analyzed. The bearing walls are similar to those of Torre Astesiano, save that the lower storeys are coated with a thick layer of plaster of over 10 cm. The thickness of the walls ranges from 1.8 m at the base to 0.6 m at the top. The square shaped structure has been incorporated in a valuable building from the Italian Art Nouveau period.

Fig. 15.13 Overall view of the medieval towers of Alba.

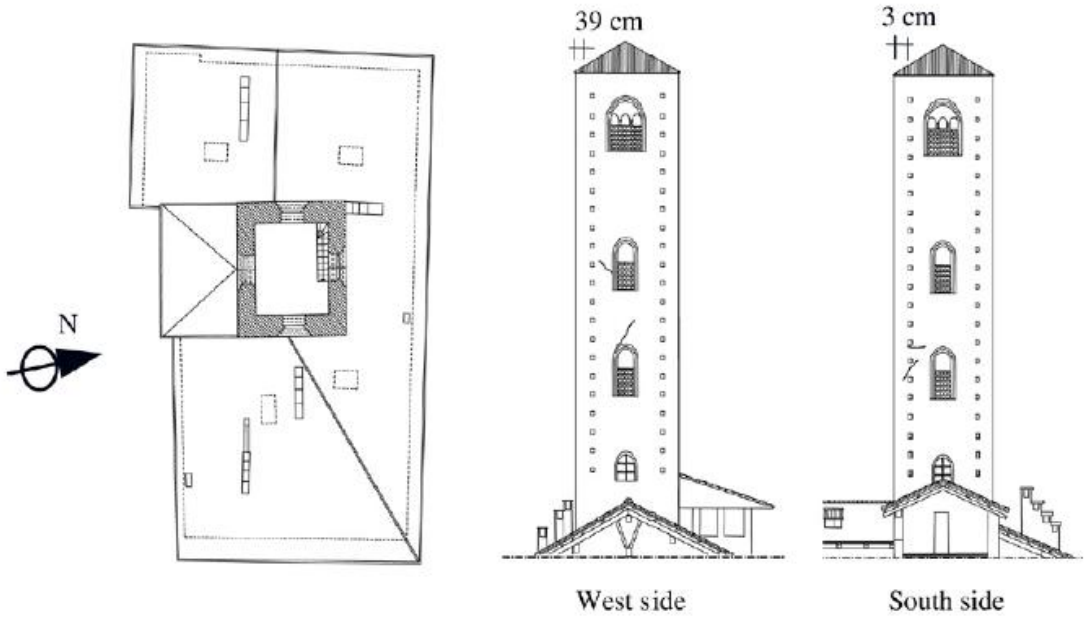

Fig. 15.14 Torre Sineo. Plan and elevations of two sides of the tower. Notice the presence of cracks near the openings and the deviation from verticality of the tower.

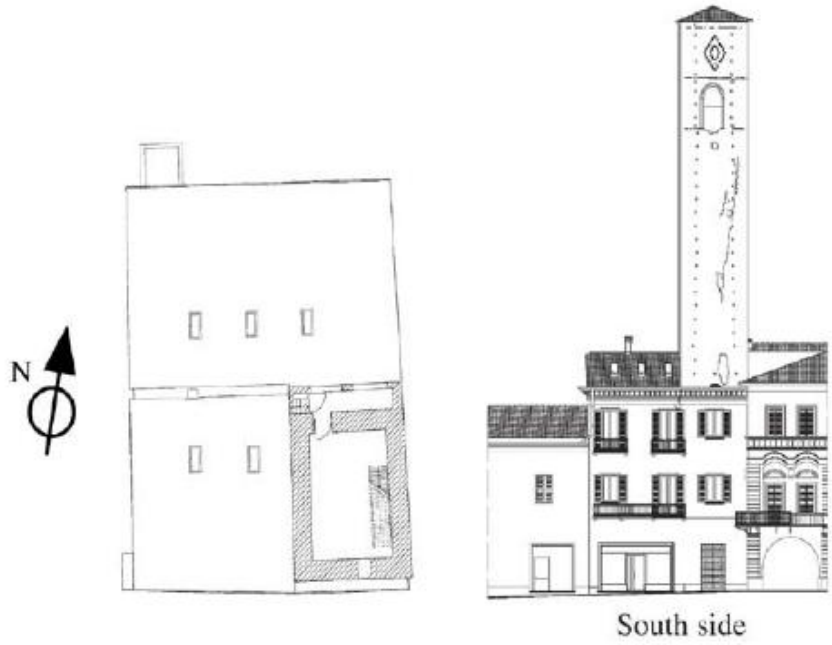

Fig. 15.15 Torre Astesiano. Plan and elevation view of the tower. Notice the presence of the main crack in the upper part of the tower.

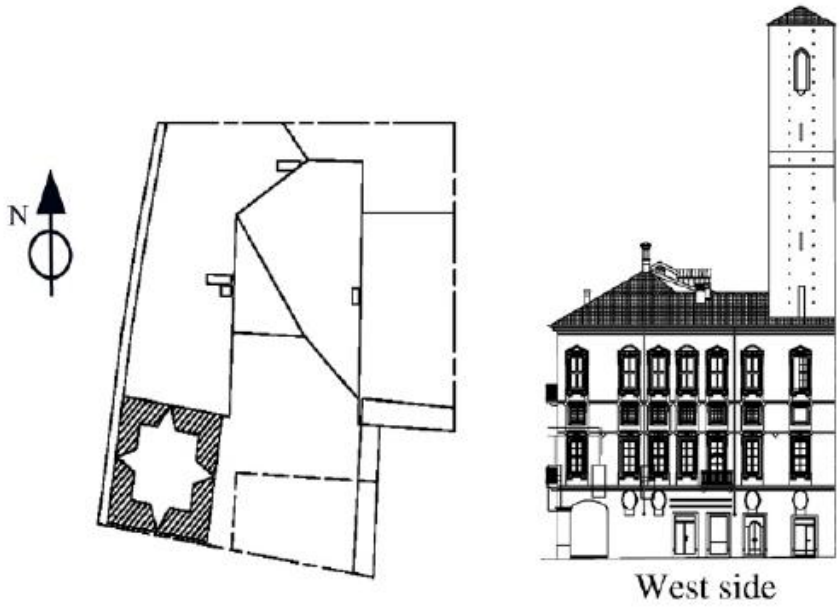

Fig. 15.16 Torre Bonino. Plan and elevation view of the tower.

The cracking pattern and the slant of the Sineo tower are schematically summarized in **Fig. 15.14**. The cracking configuration of the Astesiano Tower is not characterized by cracks distributed over the entire surface of the masonry, but rather by a long vertical crack in the upper part of the southern facade (**Fig. 15.15**). No cracks are visible in the external façade of Torre Bonino (**Fig. 15.16**), but a survey revealed the presence of openings and passageways at the different floor levels, linking the tower to the adjacent building. Created during the various restructuring works performed over the years, these openings bring about an appreciable reduction in the bearing capacity of the tower.

Tests with single and double flat-jacks were performed on the masonry walls of the towers. These tests were designed to estimate stress values in the masonry at different levels and to assess the elastic modulus and failure strength in situ. **Table 1** lists the values of mean stresses in the masonry outer leaves, and the Young's modulus as determined with flat-jacks applied to the base of the towers.

Table 1 Results from single and double flat-jack tests

Tower	Compressive stress (MPa)	Young's modulus (MPa)
Sineo	0.871	5000
Astesiano	0.480	3300
Bonino	0.592	-

For the Sineo Tower, through AE monitoring, two cracks were detected in the inner masonry layer at seventh floor level (**Fig. 15.14**). The monitoring process revealed an ongoing damaging process, characterized by slow crack propagation inside the brick walls. In the most damaged zone, crack spreading had come to a halt, the cracks having achieved a new condition of stability, leading towards compressed zones of the masonry. In this particular case it can be seen that, in the zone monitored, each appreciable crack advance is often correlated to a seismic event. In the diagram shown in **Fig. 15.17**, the cumulative AE function relating to the area monitored is overlaid with the seismic events recorded in the Alba region during the same time period; the relative intensity of the events is also shown. A similar behavior was observed for Torre Astesiano. This structure was monitored by means of two transducers applied to the inner masonry layer of the tower, at fourth floor level near the tip of the large vertical crack. The results obtained during the monitoring period are summarized in the diagram in **Fig. 15.17**. It can be seen how the damage to the masonry and the propagation of the crack, as reflected by the cumulative number of AE counts, evolved progressively over time. A seismic event of magnitude 4.7 on the Richter scale occurred during the monitoring period: from the diagram we can see how the cumulative function of AE counts grew rapidly immediately after the earthquake.

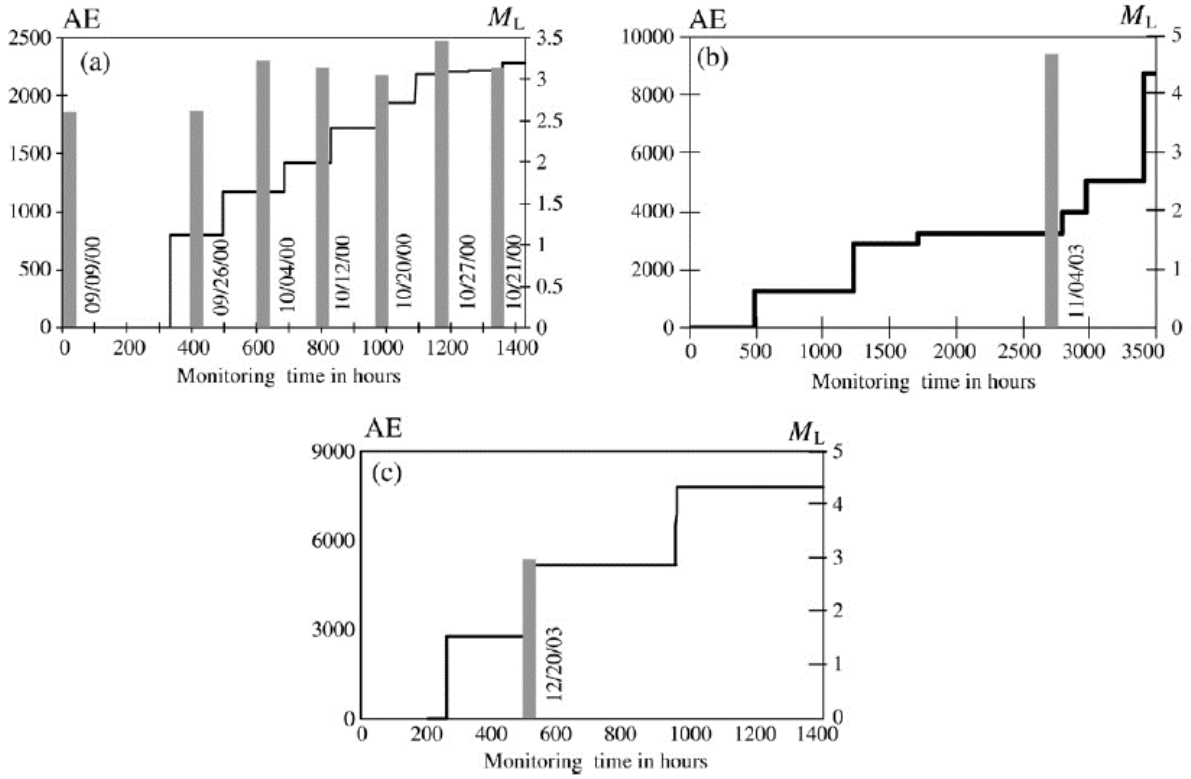

Fig. 15.17 AE counting number and seismic events in local Richter scale magnitude (ML). Torre Sineo (a), Torre Astesiano (b), Torre Bonino (c)

The monitoring of Torre Bonino was performed at first floor level, where the effects of restructuring works have affected the masonry most adversely. Under constant loading, a progressive emission of energy is observed, due to a creep phenomenon in the material. A seismic event of magnitude 3.0 on the Richter scale occurred during the monitoring period (**Fig. 15.17**). During the observation period, the towers behaved as sensitive earthquake receptors.

15.3.3 The Monte Tabor Chapel in Varallo

As aforementioned, the authors have also successfully applied the AE technique, not only to evaluate the stability of historical structures, but also to assess the state of conservation of mural painting and their structural supports. The preservation of the mural painting heritage is a complex problem that requires the use of non-destructive investigation methodologies to assess the integrity of decorated artworks without altering their state of conservation (Niccolini, Borla et al., 2014). The physical-chemical decay and the damage evolution of materials constituting the decorated surfaces and the structural masonry supports can be caused by infiltrations of water, thermo-elastic stresses, or seismic and environmental vibrations. The physical-chemical degradation has to be dealt with Materials Science and Chemical Engineering techniques (De Filippis, Tulliani et al., 2005). On the other hand, the instability and the dynamic behavior of the decorated surfaces, induced also by seismic and environmental vibrations, can be investigated by the AE technique, using monitoring systems to control continuously and simultaneously different structural supports (Carpinteri, Lacidogna, Invernizzi et al., 2013).

The data collected during the *in situ* experimental tests can be interpreted with Fracture Mechanics models and methodologies (Botvina, 2011; Botvina, Shebalin et al., 2001; Carpinteri, Lacidogna et al., 2007; Carpinteri, Lacidogna, & Puzzi, 2009). A complete diagnosis of the crack pattern regarding not only the external decorated surface but also the internal support is of great importance due to the criticality of internal defects and damage phenomena, which may suddenly degenerate into irreversible failures (Anzani, Binda et al., 2008; Carpinteri, Invernizzi et al., 2009).

The Sacred Mountain of Varallo is the most ancient Sacred Mountain of Piedmont and Lombardy and it is located among the green of the forests at the top of a rocky spur right above the City of Varallo (**Fig. 15.18**). It consists in 45 Chapels, some of

which are isolated, while others are part of monumental groups. They contain over 800 life-size wooden and multicolored terracotta statues, which represent the Life, the Passion and the Death of Christ (Niccolini, Borla et al., 2014). As the first object of investigation with the AE technique, the Chapel XVII of the Sacred Mountain of Varallo was chosen (**Fig. 15.19**). This Chapel houses the scene of the Transfiguration of Christ on Mount Tabor. The foundations were already begun in 1572, but the chapel was not completed until the 1660s. As described in (Carpinteri, Lacidogna, Invernizzi et al., 2013), also this structure has shown itself sensitive to seismic events occurring within a radius of about 100 km from the City of Varallo, and to moisture infiltrations that have the effect of detaching the mural paintings from their supports.

Fig. 15.18 The Sacred Mountain of Varallo: View of the Square of Tribunals

(a) (b)

Fig. 15.19 External view of Chapel XVII (a); internal view of the Mount Tabor installation (b)

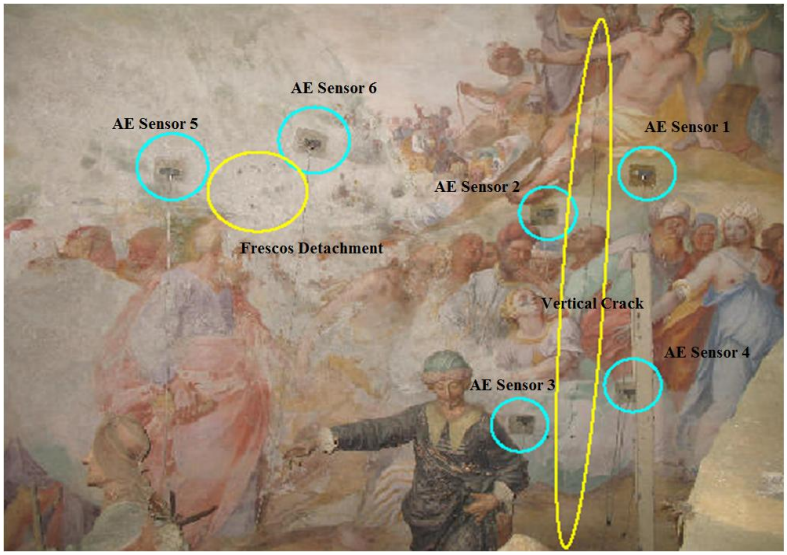

Fig. 15.20 Chapel XVII: View of the monitored damages and position of the AE sensors

As regards the structural integrity, Chapel XVII shows a vertical crack of about 3.0 m in length and a detachment of frescos, both on the North wall, which are the object of the monitoring campaign by means of AE. Six USAM AE sensors are employed to monitor the damage evolution of the structural support of the decorated surfaces of the Chapel: four are positioned around the vertical crack while two are positioned near the frescos detachment (**Fig. 15.20**). For the sensor pasting on decorated surfaces, a suitable methodology was applied. The necessary operations for bonding the AE sensors to the wall were carried out by a group of restorers that prepared a film of Japanese paper which is coated with a thin layer of "Paraloid". The "Paraloid" is an acrylic resin (methyl acrylate soluble in ketones, esters, hydrocarbons and chlorinated hydrocarbons) and is used in the field of restoration as a consolidant at low concentrations (2,4%) or as an adhesive at higher concentrations. It allows an excellent waterproof performance and has the advantage of being reversible and long-term stable. The layer of "Paraloid" forms a good protective base for the AE sensors bonded with silicone glue.

The monitoring period of the structural supports of the chapel began on April 28, 2011 and ended on June 4, 2011, it lasted about 900 hours. The results obtained by the application of the AE sensors are presented in **Fig. 15.21** and **Fig. 15.22**. For the vertical crack (**Fig. 15.21**), approximately 550 AE signals were analyzed, while for the frescos detachment (**Fig. 15.22**) 1200 AE signals were considered. The cumulated AE signals, AE rates, β_t parameters and *b*-values are shown in **Fig. 15.21** and **Fig. 15.22**. In particular, to calculate the β_t parameters and the *b*-values represented in **Fig. 15.21**, about 200 data for time were used, while about 400 data for time were used for the same parameters reported in **Fig. 15.22**. More specifically, the three *b*-values calculated for the vertical crack are shown in **Fig. 15.23** with the corresponding coefficients of determination R^2. As can be seen from **Fig. 15.21**, the vertical crack monitored on the North wall of the chapel presents a stable condition during the acquisition period ($0.5 < \beta_t < 1.0$) and the distribution of cracks on a surface domain is clearly proven by the *b*-value in the range (0.95, 1.15). In this case, it is interesting to note that, since the monitored wall is of large dimensions, a *b*-value approaching to 1 does not imply a substantial loss of load-bearing capacity of the entire wall, but rather the coalescence of the micro cracks along the surface of the vertical crack, which can continue to advance without substantially compromising the structure bearing capacity.

Further evidence for the presence of the crack is offered by the low frequency signals registered (< 200 kHz): as a matter of fact, considering the velocity as a constant and applying the Lamb ratio (Lamb, 1917), the wavelength needs to be larger than the size of the maximum inhomogeneity in order for the wave to pass through without significant modifications in its waveform. It is reasonable to assume that for a high frequency wave it is possible only to propagate through a small inhomogeneity; on the contrary for a low frequency wave it is possible also to propagate through a large inhomogeneity (Carpinteri, Lacidogna et al., 2007; Landis & Shah, 1995).

Concerning the monitored frescos detachment (**Fig. 15.22**), the decorated surface tends to evolve towards metastable conditions ($0.5 < \beta_t < 1.8$) and the signals acquired show high frequency characteristics (< 400 kHz): therefore a distribution of micro cracks in the volume is assumed for the analyzed region.

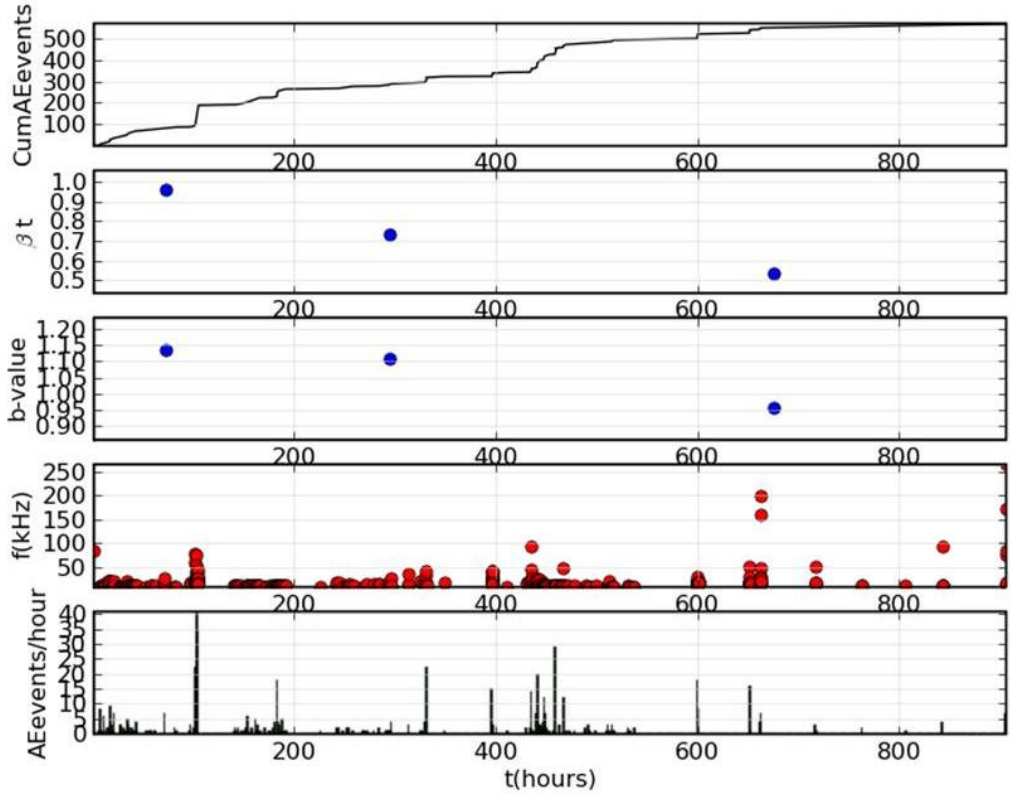

Fig. 15.21 Chapel XVII: AE from the vertical crack monitoring

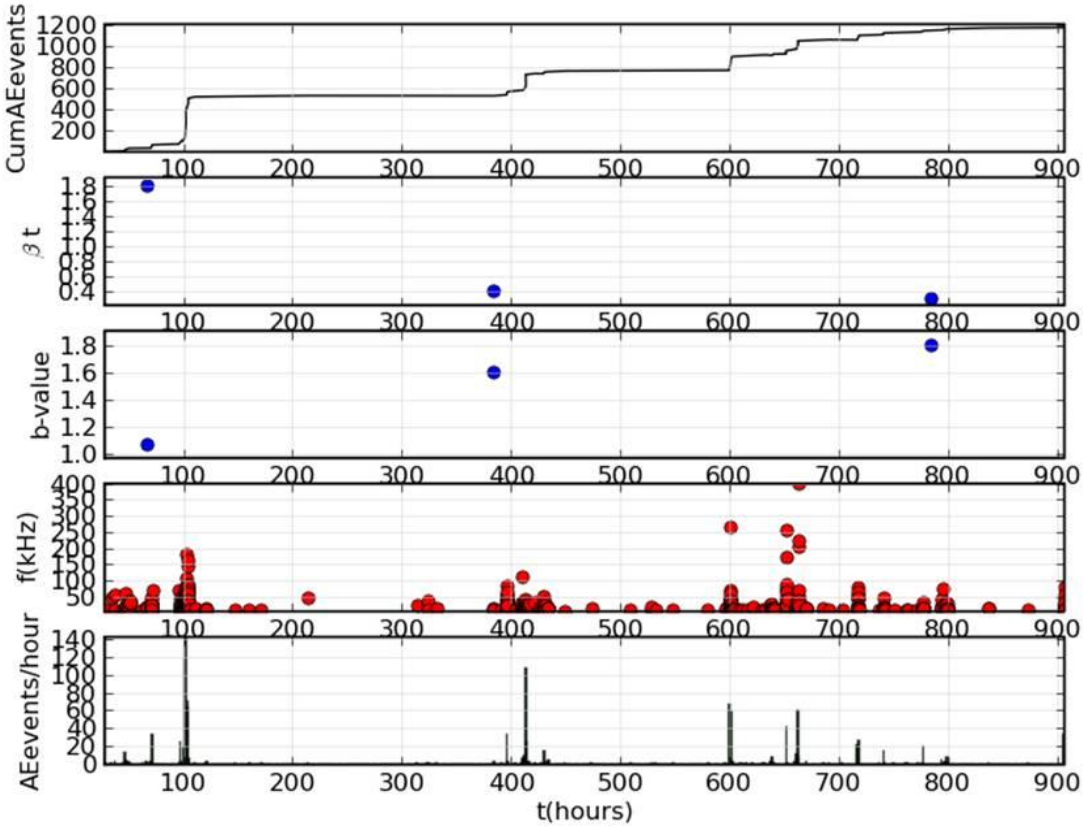

Fig. 15.22 Chapel XVII: AE from frescos detachment monitoring

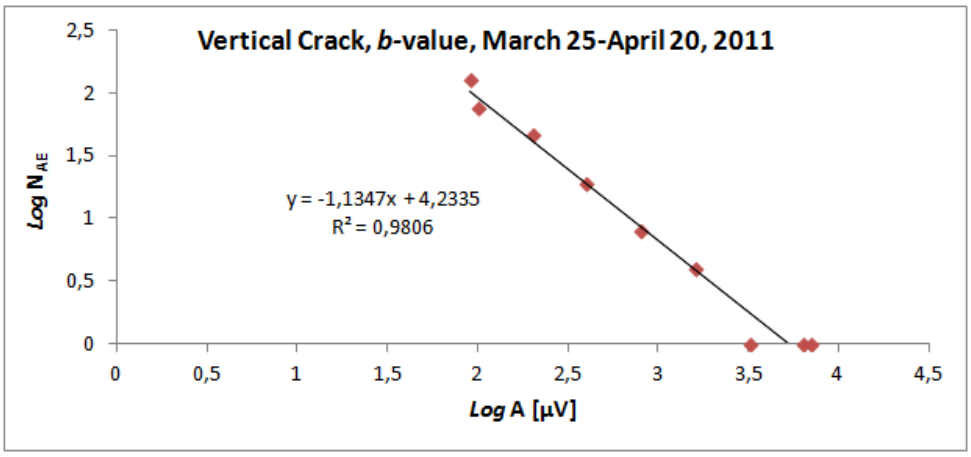

(a)

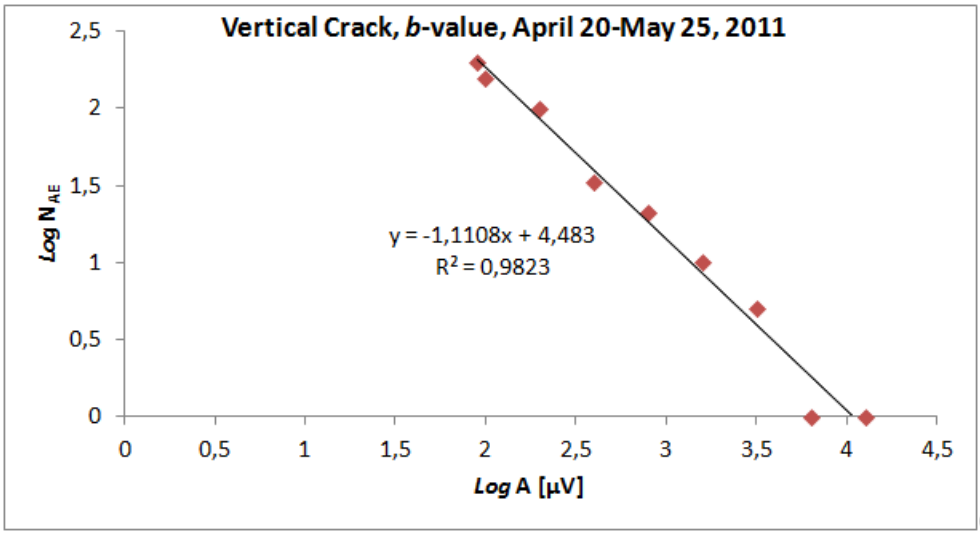

(b)

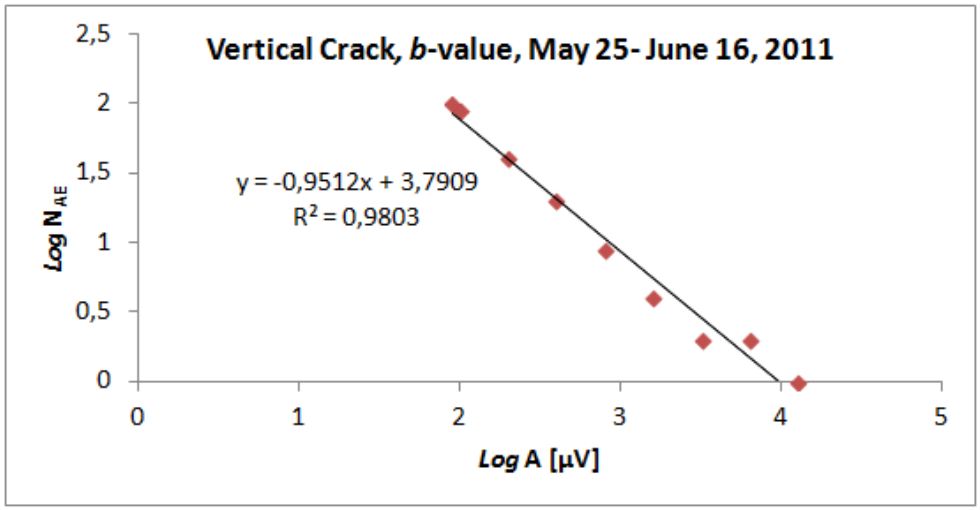

(c)

Fig. 15.23 Chapel XVII: *b*-values computed for the vertical crack with the corresponding coefficients of determination R^2; from March 25 to April 20, 2011 (a); from April 20 to May 25, 2011 (b); from May 25 to June 16, 2011 (c).

15.3.4 The Asinelli Tower in Bologna and other cases

Concerning the application of 1/*f* noise power spectra analysis, the AE technique has been employed to assess the stability of the tallest structure in the city of Bologna (Italy), the Asinelli Tower, which, together with the nearby Garisenda tower, is the renowned symbol of the city (**Fig. 15.24**) (Carpinteri, Lacidogna et al., 2016). The Asinelli Tower dates back to the early XII Century, and it is the tallest leaning tower

in Italy. The tower measures 97.30 m in height, the side is 8.00 m at the base, and 6.50 m at the top. Its leaning is of 2.38 m westward.

The AE activity in the masonry was detected in a significant region for monitoring purposes and easy to reach. Six piezoelectric sensors (working in the range of 50–800 kHz) were attached on the north-east corner of the tower, immediately above the terrace atop the arcade, at an average level of ~9.00 m above ground. In this area, the double-wall masonry has a thickness of ~2.45 m. AE monitoring began on 23 September 2010 at 5:40 p.m., and ended on 28 January 2011 at 1:00 p.m., covering, therefore, a 4-month period. The AE monitoring was carried on exploiting the USAM system. To filter out the environmental background noise a detection threshold of 100 mV was set. From the monitoring process carried out on a relevant part of this tower, it was possible to evaluate the incidence of seismic activity, vehicle traffic, and wind action on fracture evolution and damaging phenomena within the structure.

Fig. 15.24 The Garisenda Tower and the Asinelli Tower, in Bologna City center

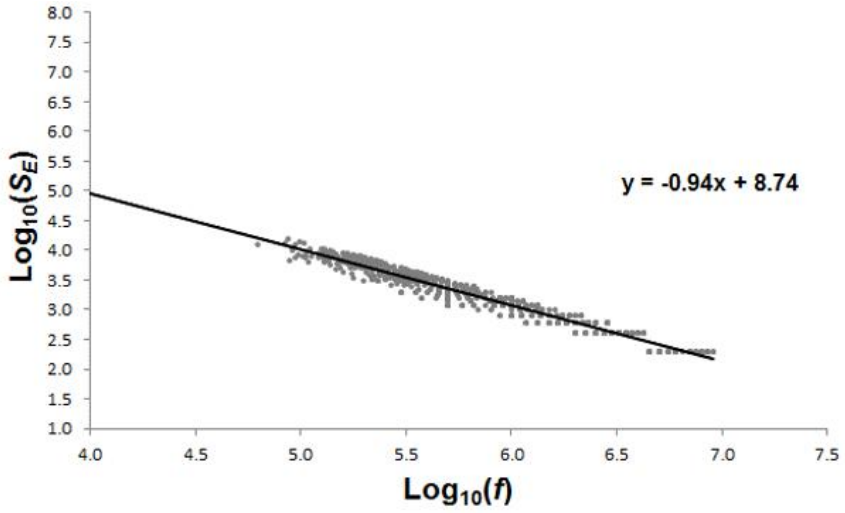

Fig. 15.25 Log-log plot of AE power spectrum versus frequency for the Asinelli Tower, Bologna: $1/f^{\gamma}$ noise, with $\gamma = 0.94$. Pink noise source (Correlated phenomena).

In **Fig. 15.25**, AE data obtained during the structural monitoring are represented in a log-log plot of power spectrum versus frequency, with a fluctuation of f^{γ} ($\gamma = 0.94$). Therefore, the source noise revealed by AE signals sounds "pink", supporting the evidences of the cracking process found during the monitoring campaigns. We can say that, in the masonry region monitored by means of AE, pink noise fluctuations suggest that the material strength has been locally exceeded.

As a second object of $1/f$ analysis, the results of the monitoring of Chapel XVII of the Sacred Mountain of Varallo are chosen (**Fig. 15.19**). The results obtained by the application of the AE sensors are represented in a log-log plot of power spectrum versus frequency (**Fig. 15.26**), with a fluctuation of f^{γ} ($\gamma = 0.92$). Also in this case, the source noise revealed by AE signals sounds "pink", supporting the evidences of the cracking process found during the monitoring campaigns.

Finally, the log-log plot of the AE power spectrum versus frequency for a monitored masonry arch, belonging to the Racconigi Castle (**Fig. 15.27**) in Piedmont (Italy) is presented. This last example is proposed in order to demonstrate that a "white"

response is obtained on a masonry structural element in which the post-peak loading phase is far from being achieved. From the results in **Fig. 15.28**, $1/f^{\gamma}$ noise is observed with $\gamma \sim 0.0$, that characterizes white sources, generated by small defects randomly diffused in the structural volume.

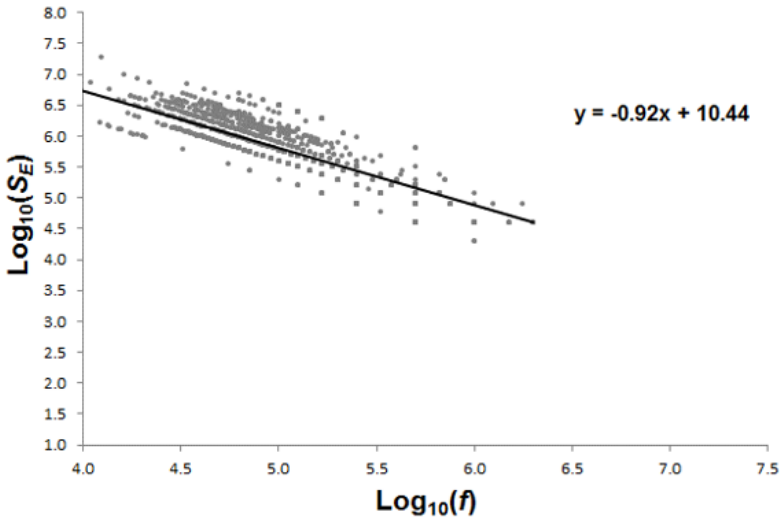

Fig. 15.26 Log-log plot of AE power spectrum versus frequency for the Chapel XVII of the Sacred Mountain of Varallo: $1/f^{\gamma}$ noise, with $\gamma = 0.92$. Pink noise source (Correlated phenomena).

(a) (b)

Fig. 15.27 External view of the Racconigi Castle (Italy) (a) and the monitored masonry arch inside the Castle (b).

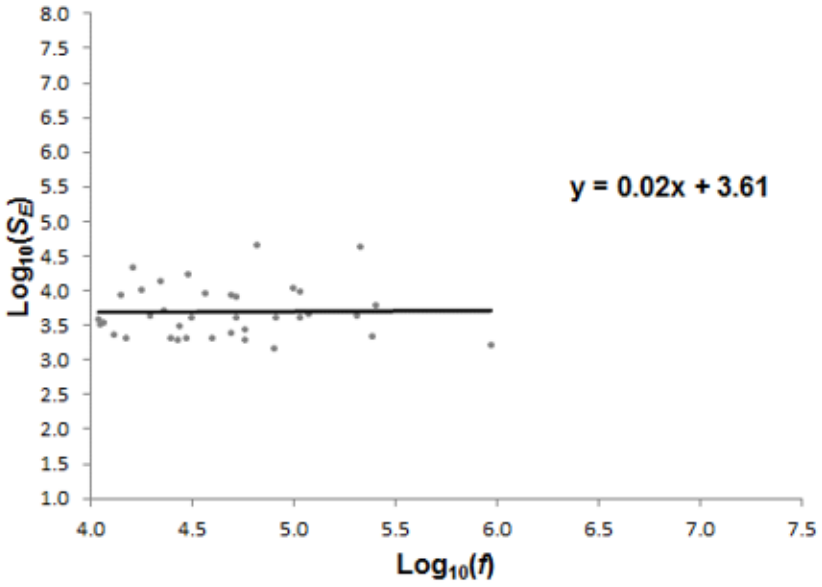

Fig. 15.28 Log-log plot of AE power spectrum versus frequency for the monitored masonry arch: $1/f^{\gamma}$ noise, with $\gamma \sim 0.0$. White noise source (Random phenomena).

It is possible to find in the previous discussion a parallel with the statistical distribution analysis of AE events, the so-called *b*-value. Therefore, the emitted energy modalities are identified during the monitoring process by determining the *b*-value variations. *b*-value extreme cases are: the critical conditions $b = 1.5$, when the energy emission takes place through small defects diffused homogeneously in the structural volume; and $b = 1.0$, when energy emission takes place throughout preferential fracture surfaces.

In the Racconigi Castle case-study, a diffused damage is observed, $2b = D = 3.0$, i.e., the cracks are distributed in a fractal domain near a volume, whereas in the Asinelli and Varallo case-studies, two-dimensional macro cracks are formed leading to the separation of some structural parts, $2b = D = 2.0$, i.e., the cracks are distributed in a fractal domain close to a surface (Carpinteri & Accornero, 2018; Lacidogna, Accornero et al., 2019). Like the *b*-value analysis, the $1/f^{\gamma}$ noise model analyzes the

transition from the diffused damage condition to that of imminent collapse, when damaging structures sound “pink”.

15.4 AE monitoring during experiments on masonry

The acoustic emission technique has shown great potential for damage detection and fracture characterization during experimental work on masonry (Anzani, Binda et al., 2008; Shetty, Livitsanos et al., 2019; A.K. Tomor & Melbourne, 2007; A. K. Tomor & Verstrynge, 2013; Verstrynge, Adriaens et al., 2014; Verstrynge, De Wilder et al., 2018; Verstrynge, Schueremans et al., 2009; Verstrynge, Wevers et al., 2016). The current section reports two successful experimental campaigns in which the use of AE sensing provided essential information to monitor and fully understand the damage progress. In the first study, AE data are applied to capture micro cracking in small masonry walls that are subjected to compressive creep and fatigue loading, and a creep failure prediction model is set up based on AE monitoring data. In the second experimental campaign, cracking in a full-scale masonry wall is monitored under cyclic loading and AE data are compared with other monitoring techniques. In both experimental campaigns, regular brick masonry and lime-based mortars are concerned, as being most relevant for historical masonry in Western Europe.

15.4.1 AE sensing during creep and fatigue testing of masonry

Fatigue and creep are both time-dependent progressive deterioration phenomena, the former under long-term cyclic loading while the latter occurs under constant loading. Compressive creep under high sustained stresses has been identified as a potential damage cause in masonry (Binda, 2008; Verstrynge & Van Gemert, 2018). Creep damage in masonry causes micro cracking, which may lead to macro cracks, and even creep failure of the masonry. The collapse of several historical towers has been attributed to creep damage accumulation (Binda, 2008; Verstrynge, Schueremans et al., 2011). Fatigue may be relevant, for example, to masonry arch bridges with

heavily increased traffic loading or to tall structures subjected to wind loading. Acoustic emission has been used for studying fatigue deterioration in masonry by Melbourne (Melbourne & Tomor, 2006), De Santis (De Santis & Tomor, 2013) and Masera (Masera, Bocca et al., 2011) under laboratory conditions and by Tomor (A.K. Tomor & Melbourne, 2007), Shigeishi (Shigeishi, Colombo et al., 2001) and Invernizzi (Invernizzi, Lacidogna et al., 2011) on vaults and masonry arch bridges. To study creep deterioration in masonry, acoustic emission monitoring has been used by Verstrynge (Verstrynge, 2019; Verstrynge, Schueremans et al., 2009) and by Carpinteri and Lacidogna (Carpinteri & Lacidogna, 2007a).

Both for creep and fatigue, damage progress is reported to occur as a three-stage process. For creep, the primary phase presents a decreasing damage rate after load application, a secondary phase with constant damage rate and, if relative stresses are considerably high, a tertiary phase in which damage accumulates into an unstable situation leading to failure of the masonry. In fatigue, the three stages are referred to as damage initiation, propagation and failure. The damage rate can be monitored by means of average strains and deformations, observed on the macro scale, but also by means of AE activity. **Fig. 15.29** indicates the good agreement between a theoretical three-phased creep curve and the cumulative AE events monitored during several uniaxial compressive creep tests on masonry samples (Verstrynge, 2010). In (Verstrynge, Adriaens et al., 2014), it was reported that the application of on-line recorded AE-data to guide the stress increase steps during an accelerated creep test on sandstone samples increased the success rate of the experiments from 10 to 90 %.

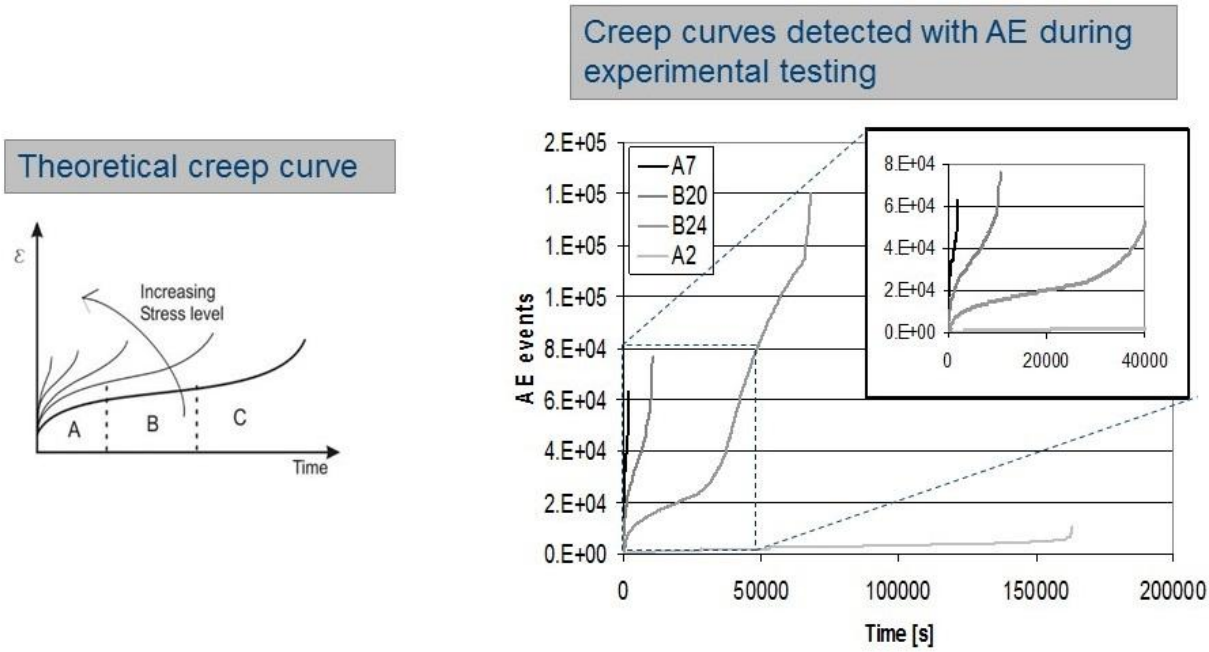

Fig. 15.29 Comparison between a theoretical creep curve (strain as a function of time) and the cumulative AE events as a function of time from uniaxial compressive creep tests on masonry samples (Verstrynge, 2010).

In the experimental program reported in this section, experimental tests on small masonry walls were performed to quantify the relation between AE activity and creep or fatigue damage. Therefore, a relation is sought between the AE activity during the secondary creep/fatigue phase, and the time/amount of cycles until failure of the masonry occurs. This relation is based on statistic considerations and "bathtub curve" theory, for which the interested reader is referred to (Verstrynge, Schueremans et al., 2009).

Simple compression tests, fatigue tests and accelerated creep tests (short-term, long-term and 1-step creep tests) were performed on small masonry columns (A. K. Tomor & Verstrynge, 2013). Fatigue tests were performed at the University of the West of England (UWE, Bristol, UK), and creep tests at the Catholic University of Leuven (KU Leuven, Belgium). In the short- and long-term accelerated creep tests, the stress

level was kept constant for a period of 3 hours and 2 months respectively in between increasing stress steps (Binda, Schueremans et al., 2008). In 1-step creep tests, a stress level of 80-90 % of the average compressive strength was applied, and kept constant until creep failure occurred in a time interval of 3-24 hours (Verstrynge, 2010). Fatigue tests were performed at 2 Hz frequency between a minimum (S_{Min}) and a maximum stress level (S_{Max}). During testing, two acoustic emission sensors were placed on opposite sides in the middle of each small masonry column. The amount of sensors per specimen was limited to allow monitoring multiple specimens at the same time. AE source localization was not aimed at. For creep tests, AE sensors with resonance frequency 375 kHz connected to a Vallen AMSY-5 system were applied, and for fatigue tests 150 kHz resonant sensors connected to a Physical Acoustics Micro-SAMOS system were used. An impression of the creep tests setups is given in **Fig. 15.30**.

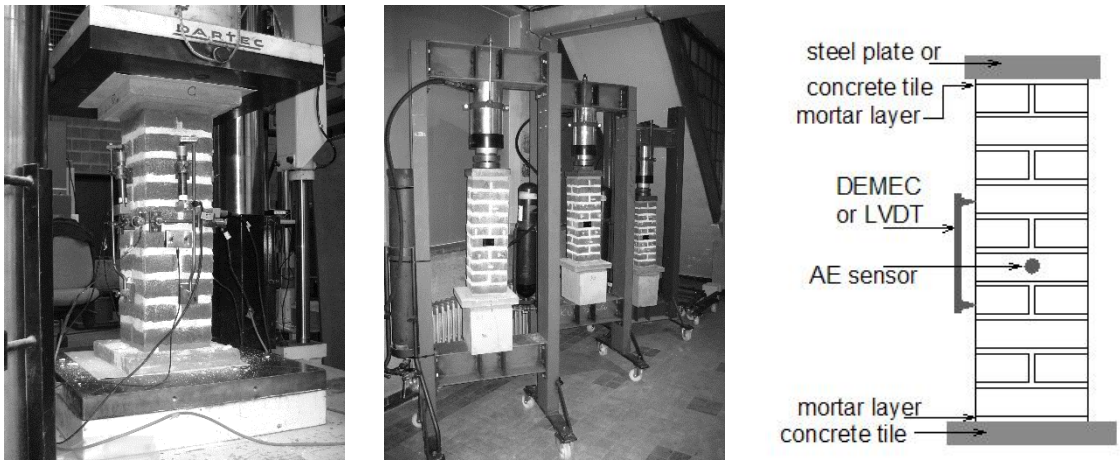

(a) (b) (c)

Fig. 15.30 (a) short-term and (b) long-term creep test setup, (c) schematic view of a masonry sample.

A typical result from a 1-step creep test and a fatigue test on small masonry columns is presented in **Fig. 15.31** and **Fig. 15.32**. Both graphs show the occurrence in time and amplitude of the AE events. For the creep test, the three creep stages can clearly be observed on the cumulative AE event curve (**Fig. 15.31**). In the beginning and towards the end of the test, larger amplitudes and energy (not shown here) are noted.

Similarly, for the fatigue test, three stages can be distinguished: initially, a relatively low, constant emission is observed (0-75% of the total number of cycles); hereafter, AE activity increases in the propagation phase showing more AE events with higher amplitude (75-95% of cycles); finally, rapid increase in emission and sudden failure occurs 95-100% of cycles (**Fig. 15.32**).

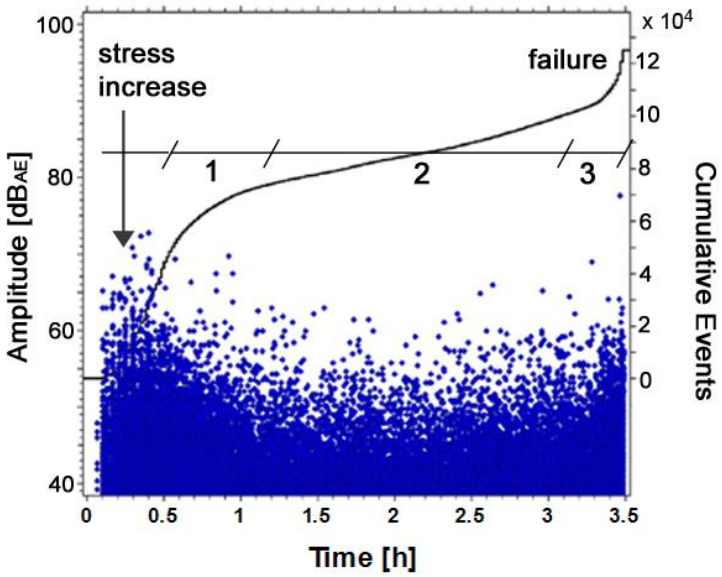

Fig. 15.31 Typical result from 1-step creep test: AE amplitude and cumulative AE event count vs. time with indicated creep phases (1, 2, 3). (A. K. Tomor & Verstrynge, 2013)

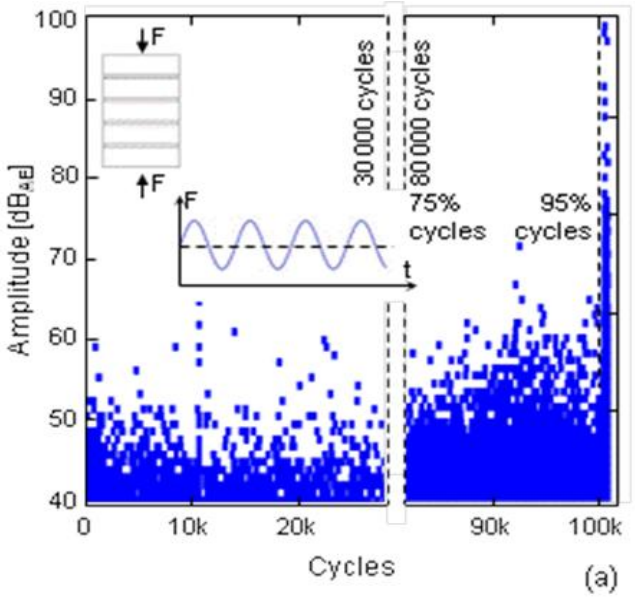

Fig. 15.32 Typical result from fatigue test: AE amplitude vs. number of cycles. A loading range between 10% (= S_{Min}) and 70% stress (= S_{Max}) was applied. (A. K. Tomor & Verstrynge, 2013)

As higher stress levels are likely to induce higher intensity micro- and macro-crack development, strong correlation is expected to exist between stress level and AE intensity. In this respect, the three-phase creep curve and more specifically the relationship between the damage rate during the secondary creep phase and stress level can be described with a Weibull distribution model. This statistical background for creep failure prediction based on AE detection was presented in (Verstrynge, Schueremans et al., 2009). **Fig. 15.33** shows the AE event rate (number of AE events per minute) during the secondary creep phase against time to failure (T). A correlation can be observed that can help identify the time to failure based on monitored AE event rate. In **Fig. 15.33**, values are presented on a double logarithmic scale that implies decreasing accuracy for increasing time to failure. In addition, prediction accuracy may reduce for lower stress levels (longer times to failure) if the AE activity is of similar magnitude as the background noise caused by fluctuating environmental conditions. The largest time interval between stress increase and failure, obtained during the laboratory tests, was approximately 2 months. Although the values in **Fig. 15.33** are only indicative of a specific masonry type and AE setup, tested under constant environmental conditions, it intends to demonstrate the general principle for prediction of creep failure in masonry based on AE data.

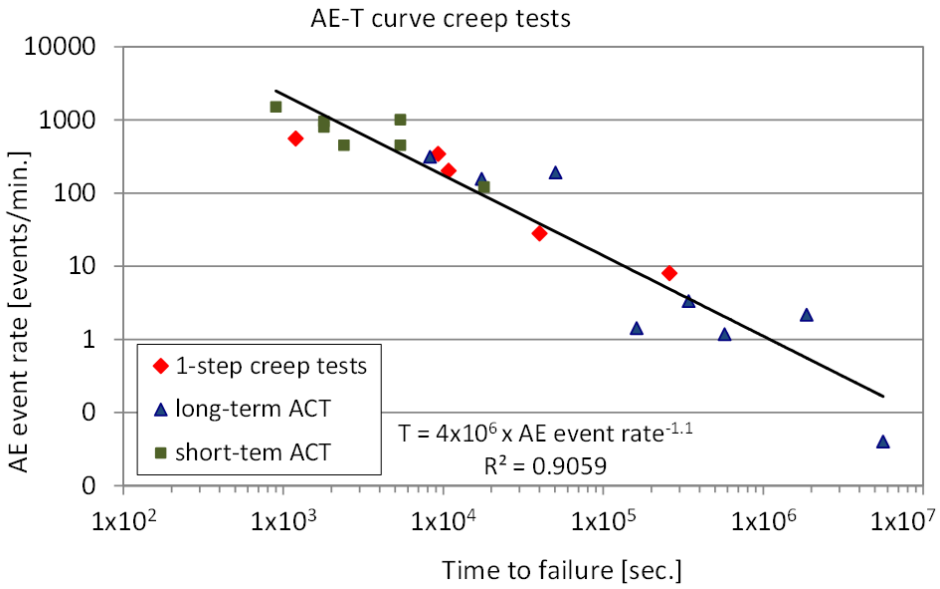

Fig. 15.33 Correlation between AE event rate (AE) during the secondary creep phase and time to failure (T) of masonry samples under uniaxial compressive creep loading.

15.4.2 Analysis of a full scale wall and comparison with other NDT

The aim of the research presented in this section is to develop techniques for monitoring of settlement-induced cracking at the scale of historical masonry walls, to obtain reliable monitoring data at the scale of a structural component that can be coupled to (settlement) data obtained at the scale of buildings and building blocks. Traditional crack monitoring devices, such as tell tales, crack width meters, LVDTs and DEMEC measurements have certain drawbacks with respect to upscaling. They can only locally detect 1D displacements, they often need to be reachable for read-outs, it is laborious to integrate them in a distributed sensor network and they cannot be integrated within the structure, thus remain visible. However, many of these techniques also have the advantage of long-term reliability and limited data drift.

In this experiment, distributed strain and acoustic wave sensing were investigated for crack monitoring in masonry. Optical fiber sensor systems are applied, which can combine the accuracy of local sensors with the advantages of distributed sensor

networks. In total, five different techniques have been applied on a full-scale masonry wall during an experimental three-point-bending test: optical fibers with distributed Fiber Bragg Grating sensors (FBG), Digital Image Correlation (DIC) without the use of a speckle pattern, optical fiber sensors for Acoustic Emission sensing (AE-FOS), piezo-electric transducers for Acoustic Emission sensing (AE-PZT) and LVDTs for displacement measurements. Only the AE sensing results are discussed here in detail, and compared with data from FBGs and LVDTs. In addition, temperature data and load-displacement data were also recorded. For a discussion on the DIC results and effect of temperature fluctuations on the measurement data, the reader is referred to (Verstrynge, De Wilder et al., 2018). For the working principles and application of optical fiber sensors for Acoustic Emission sensing (AE-FOS), the reader is referred to (Verstrynge, Pfeiffer et al., 2014).

Tests were performed on a masonry wall with dimensions 960 x 2100 x 188 mm^3, constructed with 16 courses in a Flemish bond. The wall is made of solid clay bricks with dimensions 188 x 48 x 88 mm^3 and 12 mm thick mortar layers in hybrid lime-cement mortar. Standard material testing indicated an average compressive strength of 10 MPa and 3.75 MPa for the bricks and mortar, respectively (Verstrynge, De Wilder et al., 2018). The test wall is subjected to a cyclic three-point bending test with increasing force amplitude. The masonry wall is supported on two concrete blocks, and the area between the support points is filled with polyurethane plates to support the specimen's weight and avoid falling of the test specimen after failure occurred, see **Fig. 15.34**. Sensor locations are indicated in **Fig. 15.34**. All optical fiber sensors were integrated in the bed joints of the masonry wall. The experiment is carried out in load control. Three cyclic compression tests were performed. During each test, a preload of 1 KN was applied after which the load was increased in steps of 2, 5 and 20 kN for tests 1, 2 and 3 respectively. The load was decreased after each cycle until the selected preload was again obtained. In between the three tests, the

specimen is fully unloaded during the night. During the third test, failure of the masonry wall occurred at a failure load of 76.4 kN.

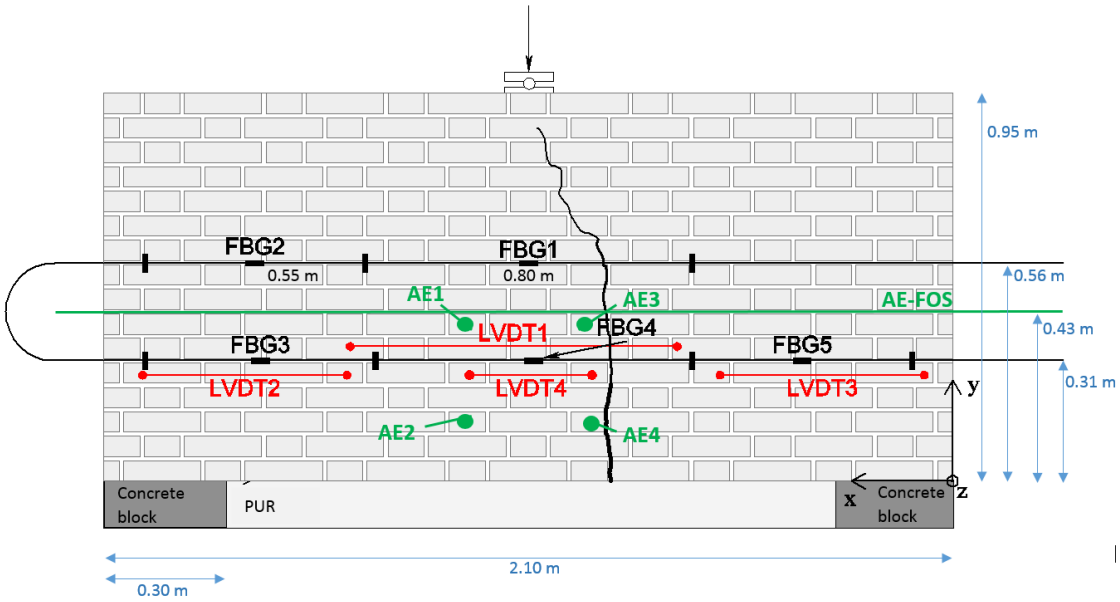

Fig. 15.34 Test setup of three-point bending test on masonry wall, with indication of the positions of sensors and the major crack that occurred at the end of test 3

During test 1, no damage was detected. The only sound results obtained from test 1 were elastic strains in the order of 5 µm/m or 0.005 ‰, which is well below the ultimate tensile strain of the masonry. Therefore, the results of test 1 are not discussed further. In test 2, no visual damage was observed. During test 3, small vertical cracks were visually observed in the mortar joint and lower bricks from a load of 60 kN. In the next load cycle, these cracks coalesced into a large macro crack (indicated in **Fig. 15.34**) after which the test was stopped. The major crack did not appear in the central (symmetric) position in the wall, indicating that asymmetry had been present in the material properties, geometry and/or boundary conditions.

Four PZT-type acoustic emission sensors were positioned in the lower middle area of the wall, at a distance of 24 cm (vertically) and 29 cm (horizontally) from each other, indicated with AE1-AE4 in **Fig. 15.34**. A threshold of 34 dB was applied for AE

event detection. Resonance type AE sensors with a peak sensitivity at 150 kHz were applied. As the maximum source-sensor distance observed in the masonry wall was limited to an average of 30 cm (depending also on the number of joint crossings), and the crack unexpectedly occurred outside of the rectangular area defined by the AE sensors' position, no accurate source location data could be obtained. Therefore, AE data are not shown as located events, but as cumulative AE energy monitored by each of the four individual AE sensors. The energy unit is defined as 1eu = 1E-14V²s. In addition, crack localization was merely based on the location of the nearest AE sensor (firstly) detecting the AE event.

Fig. 15.35 and **Fig. 15.36** present an overview of results for tests 2 and 3. The strain data, obtained from the FBG interrogation during the tests, are converted into deformations by multiplication with the base length, being the distance between the connector points of the optical fiber with the masonry. For reference, the results of the LVDTs are also presented. The observed noise level, which is related to the accuracy of the measurement, was around 2.0 µm for the LVDTs and 0.8 µm for the FBGs. Both techniques were able to capture the elastic deformations and the onset of cracking. In comparison, the FBGs demonstrated better accuracy and robustness. In each test, one out of four LVDTs (LVDT1) did not work properly due to friction between the moving and fixed parts. All FBGs performed well during the three tests and reliable deformation data were obtained, which followed the force application scheme (see **Fig. 15.35**). AE sensor 2 and 4, both located near the tension zone at the bottom of the wall clearly detect a higher AE energy level from the start of test 2 (**Fig. 15.36**). Halfway test 2, when the micro cracking localizes near sensor 4, the AE activity detected by sensor 2 falls back. In the last load step of test 2, it is likely that micro cracking has reached AE sensor 3 as an increase in AE energy is detected. In test 3, it is clear that the asymmetric macro crack is located near AE sensor 4, as this sensor detects the highest AE energy during loading, but also during unloading,

which indicates friction in the existing cracks. At the final cycle, AE sensor 3 detects the highest amount of AE events (max. values are not shown in **Fig. 15.36**).

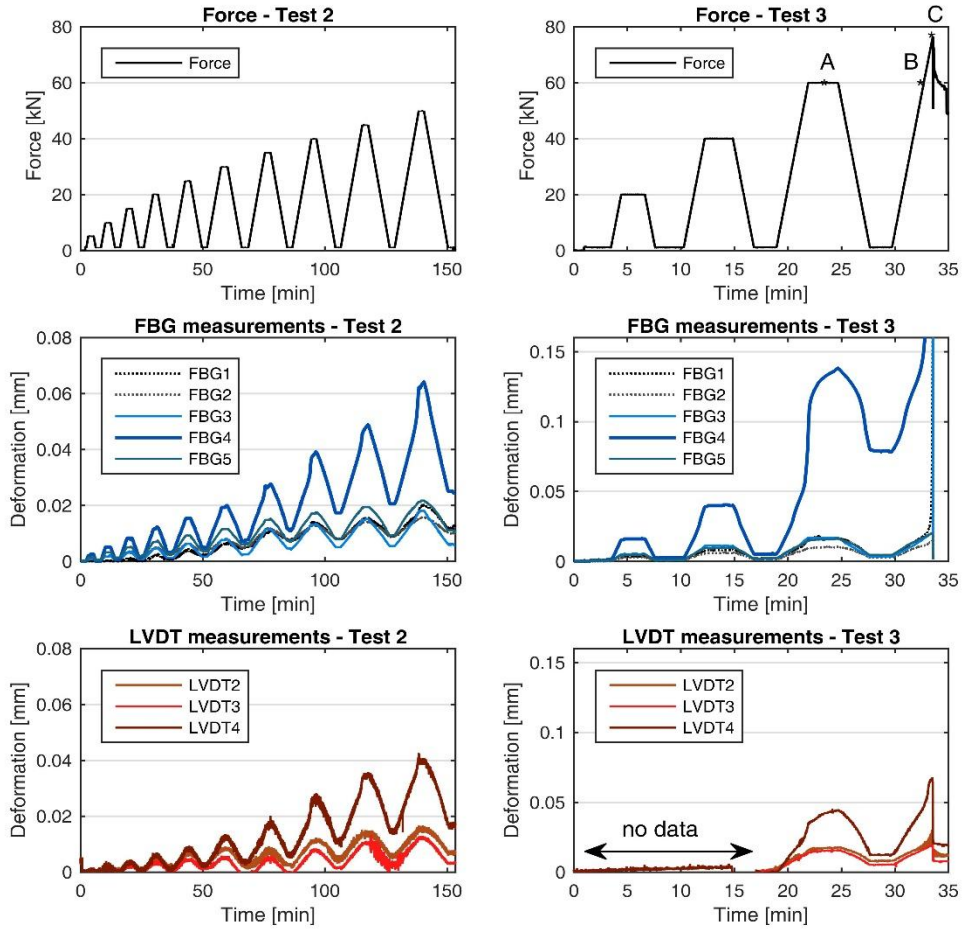

Fig. 15.35 Applied force (top), deformations measured with FBGs (middle) and with LVDTs (bottom) during cyclic three-point bending test 2 (left) and test 3 (right).

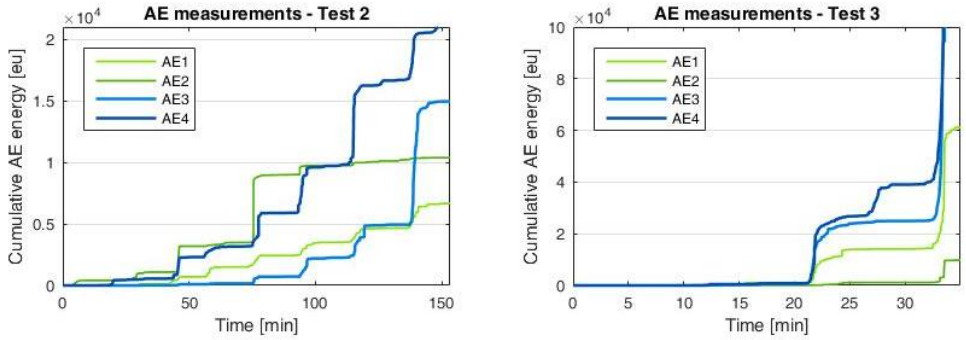

Fig. 15.36 Cumulative AE energy measured by each of the four AE sensors, test 2 (left) and test 3 (right)

The optical fiber for acoustic emission monitoring (AE-FOS) was positioned at a height of 0.43 m from the bottom of the wall, in between the two lines of FBG sensors and just above the piezoelectric AE sensors, see **Fig. 15.34**. For the masonry wall, the detection range of the AE-FOS was found to be limited to 2 cm on each side along the optical fiber and only the major cracking at the end of test 3 was detected. In previous tests on concrete beams, acoustic emissions could be successfully detected up to a range of 5-10 cm with the AE-FOS (Verstrynge, Pfeiffer et al., 2014).

In the following paragraph, it is illustrated how the Kaiser effect and Felicity ratio can be applied to support the assessment of damage progress (see also Section 15.2.2). Both effects are presented in **Table 2**, for each of the four AE sensors. The calculated values in **Table 2** are the ratios between the load level at which first AE activity is observed during a load cycle, divided by the maximum load obtained in the previous load cycle. Here, the onset of AE activity in a load cycle is arbitrarily defined as the occurrence of at least 3 AE events in a time interval of 10 seconds. The value >1 indicates that too little AE activity was registered by a sensor to determine the start of AE activity in that cycle. LOAD ratios with a value around 1.0 are representative for the Kaiser effect. Values below 1.0 are indicative for the Felicity effect and are evidence of growth and coalescence of micro cracking in the masonry. This effect is

clearly observed towards the end of test 2 for AE sensor 4, which is the sensor nearest to the final macro crack. At this point, no visual cracking had yet been observed. In **Table 2**, no values are available for the first row, as the load in this cycle remained lower than the maximum load obtained in test 1. A slight discontinuity is also observed between the last cycle of test 2 and the first cycle of test 3 in which the previous maximum load is exceeded (being cycle 3, at 60 kN). The overnight unloading of the specimen and temperature fluctuations might have caused partial crack closure and microstructural shifts which influenced the AE activity in such a way that AE activity in test 3 was observed at slightly lower load levels than expected. On the other hand, this step also coincides with the visual observation of the macro crack in the masonry. It can thus be concluded that the evolution of the Kaiser and Felicity effect in test 2 was very consistent with the macro cracking observed towards the end of test 3.

Table 2 Ratio between load at first AE activity in a cycle and maximum load during previous cycle. (sensor 4 = crack location). Severe damage is assumed for values below 0.90 (indicated in red).

	cycle	**sensor 1**	**sensor 2**	**sensor 3**	**sensor 4**
test 2	1	/	/	/	/
	2	› 1	› 1	› 1	› 1
	3	› 1	› 1	› 1	1.50
	4	1.14	1.27	› 1	1.34
	5	1.07	› 1	› 1	1.05
	6	1.08	1.10	1.20	1.04
	7	1.10	1.15	1.07	1.05
	8	1.05	1.09	1.09	0.87
	9	0.91	1.09	1.09	0.86
	10	0.95	0.90	0.99	0.86
test 3	*3*	*0.87*	*1.20*	*0.87*	*0.86*
	4	*0.67*	*0.99*	*0.58*	*0.51*

References

Aggelis, D. G., Mpalaskas, A. C., Ntalakas, D., & Matikas, T. E. (2012). Effect of wave distortion on acoustic emission characterization of cementitious materials. *Construction and Building Materials, 35*, 183-190.

Aki, A. (1981). *A probabilistic synthesis of precursory phenomena. Earthquake prediction: An international review* (Vol. 4).

Andreev, K., Shetty, N., & Verstrynge, E. (2018). Acoustic emission based damage limits and their correlation with fatigue resistance of refractory masonry. *Construction and Building Materials, 165*, 639-646.

Anzani, A., Binda, L., Carpinteri, A., Lacidogna, G., & Manuello, A. (2008). Evaluation of the repair on multiple leaf stone masonry by acoustic emission. *Materials and Structures, 41*(6), 1169-1189.

Behnia, A., Chai, H. K., & Shiotani, T. (2014). Advanced structural health monitoring of concrete structures with the aid of acoustic emission. *Construction and Building Materials, 65*, 282-302.

Binda, L. (Ed.) (2008). *Learning from Failure - Long-term behaviour of heavy masonry structures* (Vol. 23). Southampton: WIT Press.

Binda, L., Schueremans, L., Verstrynge, E., Ignoul, S., Oliveira, D. V., Lourenco, P. B., & Modena, C. (2008). *Long term compressive testing of masonry - test procedure and practical experience*. Paper presented at the 6th International Seminar on Structural Analysis of Historical Constructions, Bath.

Botvina, L. R. (2011). Damage evolution on different scale levels. *Physics of the Solid Earth, 47*, 859-872.

Botvina, L. R., Shebalin, P. N., & Oparina, I. B. (2001). A mechanism of temporal variation of seismicity and Acoustic Emission prior to macrofailure. *Doklady Physics, 46*, 119-123.

Carpinteri, A., & Accornero, F. (2018). Multiple snap-back instabilities in progressive microcracking coalescence. *Engineering Fracture Mechanics, 187*, 272-281.

Carpinteri, A., Corrado, M., & Lacidogna, G. (2013). Heterogeneous materials in compression: Correlations between absorbed, released and acoustic emission energies. *Engineering Failure Analysis, 33*, 236-250.

Carpinteri, A., Invernizzi, S., & Lacidogna, G. (2006). *AE structural assessment of a 17th century masonry vault*. Paper presented at the 5th International Seminar on Structural Analysis of Historical Constructions, New Delhi.

Carpinteri, A., Invernizzi, S., & Lacidogna, G. (2009). Historical brick-masonry subjected to double flat-jack test: Acoustic emissions and scale effects on cracking density. *Construction and Building Materials, 23*(8), 2813-2820.

Carpinteri, A., & Lacidogna, G. (2006a). Damage Monitoring of an Historical Masonry Building by the Acoustic Emission Technique. *Materials and Structures, 39*(2), 161-167.

Carpinteri, A., & Lacidogna, G. (2006b). Structural monitoring and integrity assessment of medieval towers. *Journal of Structural Engineering (ASCE), 132*, 1681-1690.

Carpinteri, A., & Lacidogna, G. (2007a). Damage evaluation of three masonry towers by acoustic emission. *Engineering Structures, 29*(7), 1569-1579.

Carpinteri, A., & Lacidogna, G. (Eds.). (2007b). *Earthquakes and Acoustic Emission: Selected Papers from the 11th International Conference on Fracture, Turin, Italy, March 20-25, 2005*: CRC Press.

Carpinteri, A., & Lacidogna, G. (Eds.). (2008). *Acoustic Emission and Critical Phenomena: From Structural Mechanics to Geophysics, selected contributions from the 6th International Conference on Fracture Mechanics of Concrete and Concrete Structures (FraMCoS-6), Catania, Italy, 22 June 2007*: CRC Press.

Carpinteri, A., Lacidogna, G., & Accornero, F. (2018). Fluctuations of 1/f Noise in Damaging Structures Analyzed by Acoustic Emission. *Applied Sciences-Basel, 8*(9).

Carpinteri, A., Lacidogna, G., Accornero, F., Mpalaskas, A. C., Matikas, T. E., & Aggelis, D. G. (2013). Influence of damage in the acoustic emission parameters. *Cement & Concrete Composites, 44*, 9-16.

Carpinteri, A., Lacidogna, G., Invernizzi, S., & Accornero, F. (2013). The Sacred Mountain of Varallo in Italy: Seismic Risk Assessment by Acoustic Emission and Structural Numerical Models. *The Scientific World Journal, 2013*, 10.

Carpinteri, A., Lacidogna, G., Invernizzi, S., Manuello, A., & Binda, L. (2009). Stability of the vertical bearing structures of the Syracuse Cathedral: experimental and numerical evaluation. *Materials and Structures, 42*(7), 877-888.

Carpinteri, A., Lacidogna, G., & Manuello, A. (2009). The b-value analysis for the stability investigation of the ancient Athena Temple in Syracuse. *Strain, 47*, 243-253.

Carpinteri, A., Lacidogna, G., Manuello, A., & Niccolini, G. (2016). A study on the structural stability of the Asinelli Tower in Bologna. *Structural Control and Health Monitoring, 23*, 659-667.

Carpinteri, A., Lacidogna, G., & Niccolini, G. (2006). Critical behaviour in concrete structures and damage localization by acoustic emission. *Key Engineering Materials, 312*, 305-310.

Carpinteri, A., Lacidogna, G., & Pugno, N. (2007). Structural damage diagnosis and life-time assessment by acoustic emission monitoring. *Engineering Fracture Mechanics, 74*(1-2), 273-289.

Carpinteri, A., Lacidogna, G., & Puzzi, S. (2009). From criticality to final collapse: Evolution of the "b-value" from 1.5 to 1.0. *Chaos Solitons & Fractals, 41*(2), 843-853.

De Filippis, E., Tulliani, J. M., Sandrone, R., Scarzella, P., Palmero, P., Lombardi Sertorio, C., & Zerbinatti, M. (2005). Analisi degli intonaci della Cappella del Calvario al Sacro Monte di Varallo. *Arkos, 12*, 38-45.

De Santis, S., & Tomor, A. K. (2013). Laboratory and field studies on the use of acoustic emission for masonry bridges. *Ndt & E International, 55*, 64-74.

Grosse, C. U., Reinhardt, H. W., & Dahm, T. (1997). Localization and classification of fracture types in concrete with quantitative acoustic emission measurement techniques. *Ndt & E International, 30*(4), 223-230.

Invernizzi, S., Lacidogna, G., Manuello, A., & Carpinteri, A. (2011). AE Monitoring and Numerical Simulation of a Two-span Model Masonry Arch Bridge Subjected to Pier Scour. *Strain, 47*, 158-169.

Lacidogna, G., Accornero, F., & Carpinteri, A. (2019). Influence of snap-back instabilities on Acoustic Emission damage monitoring. *Engineering Fracture Mechanics, 210*, 3-12.

Lacidogna, G., Manuello, A., Niccolini, G., Accornero, F., & Carpinteri, A. (2015). Acoustic emission wireless monitoring of structures, chapter 2. In M. Ohtsu (Ed.), *Acoustic Emission and Related Non-destructive Evaluation Techniques in the Fracture Mechanics of Concrete*. Cambridge: Woodhead Publishing.

Lamb, H. (1917). On waves in an elastic plate. *Proceedings of the Royal Society A, 93*, 114–128.

Landis, E. N., & Shah, S. P. (1995). Frequency-Dependent Stress Wave Attenuation in Cement-Based Materials. *Journal of Engineering Mechanics-Asce, 121*(6), 737-743.

Livitsanos, G., Shetty, N., Verstrynge, E., Wevers, M., Van Hemelrijck, D., & aggelis, D. G. (2018a). *AE source localization accuracy optimization in masonry structures*. Paper presented at the 24th International Acoustic Emission Symposium (IAES-24), Sapporo, Japan.

Livitsanos, G., Shetty, N., Verstrynge, E., Wevers, M., Van Hemelrijck, D., & aggelis, D. G. (2018b). *Numerical simulation of wave propagation in masonry*. Paper presented at the 24th International Acoustic Emission Symposium (IAES-24), Sapporo, Japan.

Main, I. G. (1991). A Modified Griffith Criterion for the Evolution of Damage with a Fractal Distribution of Crack Lengths - Application to Seismic Event Rates and B-Values. *Geophysical Journal International, 107*(2), 353-362.

Masera, D., Bocca, P., & Grazzini, A. (2011). Frequency Analysis of Acoustic Emission Signal to Monitor Damage Evolution in Masonry Structures. *9th International Conference on Damage Assessment of Structures (Damas 2011), 305*.

Melbourne, C., & Tomor, A. K. (2006). Application of acoustic emission for masonry arch bridges. *Strain, 42*(3), 165-172.

Niccolini, G., Borla, O., Accornero, F., Lacidogna, G., & Carpinteri, A. (2014). Scaling in damage by electrical resistance measurements: An application to the terracotta statues of the Sacred Mountain of Varallo Renaissance Complex (Italy). *Rendiconti Lincei Scienze Fisiche Naturali, 26*, 203-209.

Niccolini, G., Carpinteri, A., Lacidogna, G., & Manuello, A. (2011). Acoustic emission monitoring of the Syracuse Athena Temple: Scale invariance in the timing of ruptures. *Physical Review Letters, 106*(108503), 1-4.

Shah, S. P., & Li, Z. (1994). Localization of microcracking in concrete under uniaxial tension. *Aci Materials Journal, 91*(4), 372–381.

Shetty, N., Livitsanos, G., Van Roy, N., Aggelis, D. G., Van Hemelrijck, D., Wevers, M., & Verstrynge, E. (2019). Quantification of progressive structural integrity loss in masonry with Acoustic Emission-based damage classification. *Construction and Building Materials, 194*, 192-204.

Shigeishi, M., Colombo, S., Broughton, K. J., Rutledge, H., Batchelor, A. J., & Forde, M. C. (2001). Acoustic emission to assess and monitor the integrity of bridges. *Construction and Building Materials, 15*(1), 35-49.

Shiotani, T., Fujii, K., Aoki, T., & Amou, K. (1994). Evaluation of progressive failure using AE sources and improved b-value on slope model tests. *Progress in Acoustic Emission, 7*, 529–534.

Tomor, A. K., & Melbourne, C. (2007). Condition monitoring of masonry arch bridges using acoustic emission techniques. *Structural Engineering International*(2), 188-192.

Tomor, A. K., & Verstrynge, E. (2013). A joint fatigue–creep deterioration model for masonry with acoustic emission based damage assessment. *Construction and Building Materials, 43*, 575-588.

Verstrynge, E. (2010). *Long-term behaviour of monumental masonry constructions: modelling and probabilistic evaluation. PhD Thesis.* Civil Engineering Department, KU Leuven, Leuven.

Verstrynge, E. (2019). Chapter 11: Acoustic Emission testing. In B. Ghiassi & P. B. Lourenço (Eds.), *Long-term Performance and Durability of Masonry Structures - Degradation Mechanisms, Health Monitoring and Service Life Design* (1st ed.): Elsevier, Woodhead Publishing.

Verstrynge, E., Adriaens, R., Elsen, J., & Van Balen, K. (2014). Multi-scale analysis on the influence of moisture on the mechanical behavior of ferruginous sandstone. *Construction and Building Materials, 54*, 78-90.

Verstrynge, E., De Wilder, K., Drougkas, A., Voet, E., Van Balen, K., & Wevers, M. (2018). Crack monitoring in historical masonry with distributed strain and acoustic emission sensing techniques. *Construction and Building Materials, 162*, 898-907.

Verstrynge, E., Pfeiffer, H., & Wevers, M. (2014). A novel technique for acoustic emission monitoring in civil structures with global fiber optic sensors. *Smart Materials and Structures, 23*(6), 065022.

Verstrynge, E., Schueremans, L., Van Gemert, D., & Hendriks, M. A. N. (2011). Modelling and analysis of time-dependent behaviour of historical masonry under high stress levels. *Engineering Structures, 33*(1), 210-217.

Verstrynge, E., Schueremans, L., Van Gemert, D., & Wevers, M. (2009). Monitoring and predicting masonry's creep failure with the acoustic emission technique. *Ndt & E International, 42*(6), 518-523.

Verstrynge, E., & Van Gemert, D. (2018). Creep failure of two historical masonry towers: analysis from material to structure. *International Journal of Masonry Research and Innovation, 3*(1), 50-71.

Verstrynge, E., Wevers, M., Ghiassi, B., & Lourenço, P. B. (2016). Debonding damage analysis in composite-masonry strengthening systems with polymer- and mortar-based matrix by means of the acoustic emission technique. *Smart Materials and Structures, 25*(1), 015009.